Accepted Manuscript

Geological Society, London, Special Publications

The Tumey Giant Injection Complex, Tumey Hill, California (USA)

G. Zvirtes, A. Hurst, R. P. Philipp, G. Palladino & A. Grippa

DOI: https://doi.org/10.1144/SP493-2019-3

Received 12 January 2019
Revised 23 May 2019
Accepted 29 June 2019

The Tumey Giant Injection Complex, Tumey Hill, California (USA)

G. Zvirtes[1, 3]*, A. Hurst[1], R.P. Philipp[2], G. Palladino[1, 4], A. Grippa[1]

[1] *Department of Geology and Petroleum Geology, School of Geosciences University of Aberdeen, Aberdeen, AB24 3FX, United Kingdom.*

[2] *Department of Mineralogy and Petrology, Federal University of Rio Grande do Sul, Porto Alegre, AV. Bento Gonçalves, 9500, RS, Brazil.*

[3] *Graduate Program of Geoscience (PPGGEO) of Federal University of Rio Grande do Sul, Porto Alegre, AV. Bento Gonçalves, 9500, RS, Brazil.*

[4]*Dipartimento di Scienze, Università degli Studi della Basiicata, Potenza, Italy.*

**Corresponding author (e-mail: g.zvirtes@abdn.ac.uk)*

Abstract: The Tumey Giant Injection Complex (TGIC) is a regionally-developed sandstone intrusion complex emplaced into deep-water Kreyenhagen Shale (Eocene) in the San Joaquin Basin, Central California. Detailed geological mapping, stratigraphic reconstruction and outcrop description, supported by structural analysis, allowed the architectural characterisation of the TGIC. The complex is described as two main stratigraphically-constrained intervals: i) a lower interval (250m thick) emplaced into clay-rich mudrock, consisting dominantly of sills with stepped and multi-layered geometry; ii) an upper interval (200m thick) characterized by injection breccia and large wing-like intrusions (ca. 600m width x 100m high) emplaced within predominantly biosiliceous mudrock strata. The intrusions in both intervals were derived from turbiditic channel-fills intensely modified by sand fluidisation. Sandstone intrusions and fractures affecting host strata are dominantly oriented sub-parallel to the basin axis striking between NW-SE and N-S, mainly dipping to NE and forming asymmetric saucer-shaped intrusions, suggesting structurally-driven hydraulic fracturing and sand emplacement. The absence of a deep aquifer and potential sand sources underlying the complex suggests a lateral contribution of fluid flow. The TGIC occurs at a scale similar to injection complexes recognized in the subsurface and is a valuable reservoir analogue for hydrocarbon accumulations associated with sand injectites.

Keywords: giant sand injection complex; San Joaquin Basin; intrusion geometry; intrusion architecture; injection breccia; subsurface analogue.

Giant sand injection complexes form when regional hydraulic fracturing in the shallow subsurface promotes sand fluidisation and injection. The hydraulic fracturing typically occurs in fine grained host strata, and coincides with the presence of depositional sandstone (parent units) from which sand fluidises and injects (Vigorito & Hurst 2010; Hurst *et al*. 2011). Giant sand injection complexes are significant in petroleum systems because parts of them are known hydrocarbon reservoirs (Dixon *et al.* 1995; Hurst *et al.* 2005; Briedis *et al.* 2007; Hurst & Cartwright 2007; Hurst *et* *al*. 2007; Braccini *et al.* 2008; Huuse *et al.* 2010). They form intrusive traps (Hurst et al. 2005), in which associated stratigraphic traps may occur (Hurst et al. 2006; Cobain et al. 2017), form highly permeable conduits for fluid migration (Jenkins 1930; Hurst et al. 2003a) and may act as seal breaches (Cartwright *et al.* 2007). Large-scale sandstone intrusions are described from the North Sea (Paleogene), where they are identified as significant reservoirs (Dixon *et al.* 1995; MacLeod *et al.* 1999; Bergslien, 2002; Duranti *et al*. 2002; Huuse & Mickelson 2004; Huuse *et al*. 2005; Szarawarska *et al*. 2010) and are increasingly recognized in petroleum provinces globally (Huuse et al. 2010).

Regionally developed hydraulic fractures require a sealing lithology (host unit) and a rate of ingress of a very large (unconstrained) volume of pore fluid that greatly exceeds the transmissivity of the seal (Vigorito & Hurst 2010; Hurst *et al*. 2011). Poor consolidation typifies host strata and parent units in very shallow (200-500m) burial, and small changes in hydrostatic or lithostatic gradient create supra-lithostatic pore-fluid pressure (Jolly & Lonergan 2002; Hurst *et al*. 2011). When hydraulic fractures form, they are held open by pore fluid pressure, and as flow velocity rises, transmit fluidised sand into the fractures (Hurst *et al.* 2003b; Vigorito & Hurst 2010). With the exception of features large enough to be imaged on seismic, subsurface data provide limited insight into the presence of hydraulic fractures unless continuous core recovers micro-fractured mudstone. Even steep (>40° to bedding) vertically and laterally extensive fractures with sandstone fills (dykes) are rarely detected (Grippa et al. 2019). Because of this, outcrop analogues are particularly valuable, both to provide guidance regarding diagnostic characteristics, and spatial data at higher resolution than subsurface data, while at a similar lateral and vertical scale.

Underestimation of petroleum resources in sandstone intrusions is commonplace, and attributed largely to the lack of resolution and detection of seismic data (Huuse et al. 2007; Skjaerpe et al. 2018; Satur et al. *this volume*). Although descriptions of high-quality outcrop of sandstone intrusions is increasingly common (Boehm & Moore 2002; Hubbard *et al.* 2007; Parize *et al*. 2007; Surlyk *et al.* 2007; Thompson *et al*. 2007; Scott et al. 2009; Cobain et al. 2015), most of these have limited lateral and vertical extent. One of the aims of this study is to provide detailed outcrop data of the Tumey Giant Injection Complex to better understand its genesis and evolution, and to support interpretation of subsurface data by identifying and characterising detailed geometric and architectural relationships between sandstone intrusions, parent units and host strata. At Tumey Hill, the Tumey Giant Injection Complex (TGIC) emplaced in the Kreyenhagen Shale of the San Joaquin Basin (Fig. 1) during the late Eocene has an exposed vertical thickness exceeding 450 m and extends laterally up to 4 km (Fig. 2). This facilitates accurate characterisation of stratigraphic architecture, the geometry and structure of sandstone intrusions, and their relationship to host strata and depositional parent units. In this research the detailed mapping and interpretation of the outcrop of the TGIC allowed (1) the reconstruction of the complex architecture, (2) the definition of the structural organization of the intrusive network, (3) the evaluation of the geological conditions which controlled the priming and trigger mechanisms that led to overpressuring of parent units, subsequent hydraulic fracturing of host strata, and sandstone intrusion, and (4) the assessment of the TGIC as a giant injection complex reservoir.

Geological Setting

The TGIC is exposed discontinuously along the eastern flank of the California Coast Ranges for approximately 20 km between Monocline Ridge on the south and Tumey Hills on the north (Fig. 1). The Kreyenhagen Shale (KS), within which the TGIC developed, is part of the Great Valley Group (GVG) (Ingersoll 1982) which was deposited following the Nevadan orogeny in the Late Jurassic to Oligocene as a N-S elongate forearc basin (Dickinson 1981; Ingersoll 2008). It developed in an Andean-style convergent margin setting (Graham 1987) with an arc-trench system created by the subduction of the oceanic Farallon plate under the continental North American plate to the east (Atwater 1970; Atwater & Stock 1998), forming the Sierran magmatic arc and the Franciscan subduction complex developed to the east and west of the basin, respectively (Fig. 1a and 1b).

The Tumey Hill area (Figs.1c and 2) consists of Upper Paleocene to Miocene marine and non-marine strata with several unconformities associated with tectonic pulses and sea level fluctuations

(Bartow & Nilsen 1990; Bartow 1991). It is part of the deformed western margin of the San Joaquin Basin, structured in a regionally asymmetric synclinorium with a steep western limb dipping at 30-50° to west and a gently dipping eastern limb (Ernst, 1983). The present structural configuration of the western flank of the San Joaquin Basin consists of an extensive array of NW-SE trending *en échelon* folds (Bartow 1996; Dickinson 2002) that form alternating anticlines and synclines often underlain by thrust planes (Namson & Davis 1988; Bartow 1991) (Fig. 1c and 2).

The oldest unit cropping out in Tumey Hill (Fig. 1c) is the Moreno Formation (Anderson & Pack 1915), which consists of an Upper Cretaceous to Lower Paleocene sequence of mudstone and channelized turbiditic sandstone deposited in slope and shelf-edge setting (Payne 1951; McGuire 1988), hosting the Panoche Giant Injection Complex (Vigorito *et al*. 2008; Vigorito & Hurst 2010). The top of Moreno Fm. is eroded by a regional unconformity overlain by the Lodo Formation (Late Paleocene to Early Eocene), which consists of grey claystone and siltstone and arkosic sandy turbidites interpreted as submarine fan deposits in a moderately deep basin, likely related to a trench-slope basin with palaeocurrent predominantly toward NW (Nilsen *et al.* 1974). During the Middle Eocene, the San Joaquin Basin shoaled and the coastline prograded depositing the shallow-marine deltaic and estuarine sediments of the Domengine Formation (Slagle 1979; Todd & Monroe, 1968; Schulein 1993; Sullivan & Sullivan 2012). Locally, the Domengine Formation records the collapse of the shelf by slope failure events (Sharman *et al.* 2017). Abrupt subsidence and basin-wide transgression led to the return of deep-marine conditions over most of the GVS (Milam 1985) resulting in widespread deposition of the Kreyenhagen Shale (Middle to Late Eocene) (Figs. 2 and 3).

The Kreyenhagen Shale, first defined by Anderson (1905), is a transgressive marine bathyal succession of siliciclastic and biosiliceous mudstone and shale, intervals of porcelanite and diatomite, and isolated and localised deep-water channelized turbiditic sandstone (Milam 1985) deposited in a submarine slope environment at middle to upper bathyal-outer neritic depth (Phillips *et al*. 1974). The Kreyenhagen Shale is an important hydrocarbon source rock in the San Joaquin Basin (Lillis & Magoon 2007; Peters *et al*. 2007a, b) and was recently the focus for exploitation as an unconventional oil play (OilVoice 2013). The laminated character of some strata, and the total organic carbon content (Lewan *et al.* 2014), indicate deposition under low-oxygenation sea-floor conditions associated with an oxygen-minimum zone (Milam 1985; He *et al*. 2014). The mudstone and biosiliceous mudstone are the host strata for the TGIC (Figs 2 and 3), with sandstone intrusions associated with different modes of emplacement throughout the evolution of the injection complex (Palladino et al., 2016, 2018). A significant erosional unconformity truncates the top of KS and the upper portion of the TGIC and forms the depositional surface upon which the 10-30 m thick Tumey Sandstone Lentil (Late Eocene) was deposited (Zimmerman 1944).

Data acquisition and processing

Stratigraphic relationships and structural configuration of the TGIC and its elements were mapped using a combination of satellite image analysis (Google Earth and Quickbird), detailed geological mapping, construction and correlation of sedimentary logs, and structural analysis, including facies analysis and geometric characterization of sandstone intrusions, parent units, and hydrofractured host strata.

Sedimentary logs

Sandstone body geometry and stratigraphic intervals of the TGIC were mapped, photographed, and logged throughout the Tumey Hill area (Figs. 4 and 5). Sedimentary logs played an important role in differentiating between depositional and intrusive facies, and in the definition of the stratigraphic organization and architecture of sandstone intrusions (Figs. 3 and 4). Recognition of features that facilitate differentiation between depositional (parent) units and low-angle to bedding intrusive sandstone (e.g. sills) was prioritised (cf. Duranti and Hurst, 2004; Hurst et al., 2011) (Table 1). Logs give an immediate visual impression of the sedimentary and intrusive succession (Scott *et al.* 2013; Ravier *et al.* 2015), and are a convenient way of making correlations and comparisons between equivalent sections from different portions of the complex. In order to contextualize the significant thickness variations, internal structures, and orientation of the sandstone intrusions, the sedimentary logs were integrated with a regional map, photomosaic analysis and structural interpretation. This facilitated a regional summary illustrating the most representative facies associations and geometries of the TGIC (Figs. 4 and 5).

Structural analysis

The fundamental objective of the structural analysis was to describe accurately the structural configuration of the sand injection complex, in order to define its architectural organization and spatial distribution, and ultimately characterize the relative stress field during sand injectite emplacement. Structural data collection included measurement of strike and dip orientation of bedding, fractures, folds, faults, and the orientation of sandstone intrusions (dykes and sills, and wing axes). The data collected were statistically analysed to characterize preferred orientations along with other parameters (thickness, spacing, distribution, and aperture) of intrusive bodies. Stereographic projection used Stereonet® to help in the visualization of three-dimensional orientation of the structural data.

It was assumed that at the time of sand injection event the dip of the host strata was probably close to horizontal, with a slope angle <5° roughly plunging to west and southwest (palaeo-slope). As the study area has been subject to tilting and folding by post-injection contractional deformation, it was necessary to correct the tectonic effect by a back-rotation of the bedding of 30° clockwise along a N150-trending horizontal axis. Back-rotation allowed reconstruction of the original palaeo-structural framework of the injection complex, thus establishing an accurate spatial distribution of the sandstone intrusions and associated fractured host strata at the time of sand injection.

Palaeo-stress analysis was undertaken using a similar method to that of Boehm & Moore (2002), analysing the overall orientation and dilatational directions of sheet-like intrusive bodies, in order to define the eigenvalues and eigenvectors for the distribution of all intrusions (Fig. 16a). The three principal eigenvectors and eigenvalues are an orthogonal set of axes best approximating the maximum, intermediate and minimum concentration of points in the stereoplot of poles to intrusions and to fractures, calculated by the Bingham method (Fisher *et al.* 1987). Once the attitude of sandstone intrusions and fractures, and dilation direction of intrusive sheets had been determined, it was possible to define the relative minimum (σ3) intermediate (σ2) and maximum (σ1) compressive stress vectors affecting the injection complex.

Results

Architectural organization of the TGIC

At Tumey Hill the TGIC crops out along a stratigraphic section *ca*. 450 m thick covering an area of approximately 4 km^2 (Figs. 2 and 4). We assume that the deepest portion of the complex was at least ca. 470 m below the palaeo-seafloor, an estimate that accounts for the 450m thickness of the complex below a minimum erosion of ca. 10-20 m by the overlying Tumey Sandstone Lentil, marking a late Eocene to early Oligocene unconformity which is the datum for the top of the TGIC (Fig. 5). The TGIC is defined in two distinct intrusive intervals characterized by different intrusive network geometry, parent unit`s size and distribution, and host rock composition and fracturing style. The general characteristics of the complex are summarized at Table 2.

Sandstone intrusions emanate from two main intervals of isolated, stacked sand-rich turbiditic channels defined as the lower and upper parent units (Fig. 3). The lower parent units occur intercalated with mudstones at between 300 to 470 m below the erosional unconformity and the upper parent units concentrated at 100 to 200 m below that datum (Fig. 5). Most of the sandstone intrusions occur as interconnected tabular dykes and sills and other irregular intrusion emanating from the parent units. Both dykes and sills display non-systematic cross-cutting relationships, which suggests that they were emplaced in a single injection event as observed in the PGIC (Vigorito *et al*. 2008; Vétel & Cartwright 2010; Vigorito & Hurst 2010). However other minor sand remobilization and injection occurred after the main injection event associated with extensional and contractional tectonics (Palladino et al., 2016; Palladino et al., 2018). Gypsum-filled veins crosscut the sandstone intrusions as a result of post-sand injection fluid migration and precipitation.

Lower intrusive interval

The lower intrusive interval comprises three main elements:

(i) host strata consisting of *ca*. 250 m of brown clay-rich mudstone intercalated with minor thin layers of biosiliceous mudstone (0.05-1 m thick);

(ii) parent units which consist of tabular and channelized turbiditic sandstone intensely modified by sand fluidisation;

(iii) a sill-dominated intrusive network connected by low-and high-angle dykes.

Lower Parent Units. Stacked turbiditic sandstone channel-fills, typically 1-4 m thick but up to 8 m, made up of grey, poorly- to moderately-sorted arkosic litharenite with subsidiary pebbly sandstone and conglomerate at the base of the deposits (Fig. 6). Decametric intervals of brown mudstone commonly alternate with the individual channels (Fig. 5). The lateral extent of channels is not well exposed but they are at least tens of meters wide. The arkosic litharenite is rich in volcanic, sedimentary (chert and mudrocks), and low grade metamorphic clasts, with pervasive gypsum cementation. Medium-grained sand predominates but pebbly sandstones and matrix- and mudstone clast-supported conglomerates often occur along the base of channels with sub-parallel and low angle cross stratification (Fig. 6).

Disruption of primary sedimentary structures is common (Fig. 6f-i) forming structureless units similar to the facies B3 of Duranti & Hurst (2004) that are interpreted to have formed as a result of sand fluidisation. Adjacent to the upper margins, mud-rich laminae define crudely margin-parallel banding (Hurst *et al.* 2011) with development of upward erosive surfaces into the overlying mudstone (Fig. 6d). In the central area of outcrop in figure 6a and 6b, a sandstone dyke emanates upward from the parent unit (Fig. 6e) confirming the genetic relationship between the turbiditic deposits and sandstone intrusions. Fluidisation features are abundant and easy to recognize when dykes crosscut host mudstone reaching the base of an overlying turbiditic channel (Figs. 6h and 6i). In this case the fluidised sand from the dyke was injected into the host turbidite disrupting its primary sedimentary structures such as the plane-parallel bedding, generating massive (structureless) sandstone.

Lower Intrusive Network. Sandstone intrusions emanate from the lower parent units and form a *ca*. 250 m thick intrusive interval that can be traced laterally for more than 1 km (Figs. 5 and 7). This intrusive system is sill-dominated with connecting planar and irregular (bulbous and curved) dykes (Fig. 7). Sills commonly have discontinuous tabular external geometry with erosive lower and upper margins, and individually are up to 4 m thick but typically occur in the range of 0.5 to 2 m (Figs. 7 and 12). Generally, intrusive contacts have sharp angular changes in orientation over short distances with close to perpendicular offsets of contacts on a 0.1 to 1m scale.

Short, high- and low-angle dykes <1 m thick, typically showing a thickness range between 0.2 and 0.5 m, link sill segments resulting in the formation of multi-layered sills (*sensu* Vigorito & Hurst 2010) that can reach up to 15 m thick and extend laterally for >150m (Fig. 7). Sills commonly bifurcate, taper, step and pinch-out laterally and have rapid lateral changes in thickness often splitting and, or, merging with other sills (Fig.7a, b). Sill margins are planar (Fig. 7e, f) and curved (Fig. 7c, d, g) thus recording brittle fracture and subsequent erosion of the host strata. Internally, sills commonly contain rafts of mudstone derived from the host strata (Fig.7e, f), and develop banding and irregular structures associated with sand injection (cf. Duranti & Hurst 2004; Hurst *et al*. 2011). Dykes are discontinuous, volumetrically smaller, and more irregular than the sills (Fig. 7b). They have co-occurring low and high angle planar and curved margins. Dykes split and bifurcate laterally and upward (Fig. 7d) with sub-vertical branches recording upward fracture propagation (cf. Pollard 1973). Overall, the thickness of the lower intrusive network thins upward above the lower parent units (Fig. 12).

The transition from the lower intrusive interval to the upper intrusive interval was defined as the level at which there is a change in geometry of the sandstone intrusions associated with channels was observed, from predominantly sill-dominated to wing-like intrusions and laterally extensive mudstone-clast injection breccia zone (Figs. 4 and 5). From the lower to the upper intrusive interval the composition of the host strata changes from brown clay mineral rich mudstone to very pale grey biosiliceous mudstone (Fig. 3).

Upper intrusive interval

Three main elements define the upper intrusive interval:

(i) host strata made up of brown clay-rich mudstone (ca. 50m thick) overlaid by biosiliceous-dominated mudstone (ca. 150m thick);
(ii) parent units comprising channelized turbiditic sandstones intensely modified by sand fluidisation;
(iii) an intrusive network comprising interconnected sills and dykes intruding ca. 200m thickness of host strata extending laterally for more than 2km forming an intrusive network of asymmetric saucer-shaped complexes with large-scale wing-like intrusions and injection breccia zones.

Upper Parent Units. Parent units in the upper intrusive interval are texturally and compositionally very similar to the lower parent units, but geometrically they comprise broader (up to 300m wide) and thicker (10 to 45m) isolated turbiditic channel-fill (Figs. 5, 8 and 9). Where depositional structures occur, the channels commonly have large-scale sets of cross-bedded sandstone with pebbly sandstone and conglomeratic basal lags (Figs. 8c, d). Conglomeratic lags include rounded to angular clasts of mudstone individually up to 50 cm in diameter but typically in the range of 5 to 10 cm (Fig. 8d). The channel-fills fine upward into fine- to medium-grained sandstone with massive and parallel bedding (Fig. 9). No overbank deposits were recorded. Palaeocurrent inferred from cross-bedding of these deposits indicate a crudely W-NW sedimentary transport (Fig. 5) within a NE-SW to E-W channel axis system perpendicular to the palaeo-slope of San Joaquin Basin during the deposition of Kreyenhagen Shale.

The unstructured massive sandstone in the central and upper portions of the channels is associated with intense sand fluidisation, similar to the lower parent units, creating structureless sandstone facies with irregular and chaotic fabric and, in the upper portion of the channel, fluidisation banding (Fig. 9). Fluidised sand that emanated from the upper parent units (Figs. 8b and 10) was injected laterally and vertically forming a complex system of stepped and staggered sills, and dykes (Figs. 10 and 11) within intensely hydrofractured and brecciated mudstone and biosiliceous mudstone succession forming the upper intrusive network.

Upper intrusive network. Unlike the lower intrusive network, sandstone intrusions in the upper intrusive interval predominantly consists of composite dykes, sills and irregular intrusive bodies, associated with breccia zones that are particularly well developed in biosiliceous mudstone and in proximity to the large parent beds (Figs. 5, 13 and 14). These interconnected injections commonly form asymmetric saucer and wing-like intrusions that emanate from adjacent parent units (Figs. 8b and 10).

At the Half Dome outcrop (Figs. 4, 10 and 11), a single large aperture (up to at least 12 m thick) composite intrusion forms an wing intrusion (*sensu* Huuse *et al.* 2007). The wing crosscuts more than 100 m of host strata in a series of steps with associated dykes and sills that bifurcate and merge, and extend laterally for more than 600 m from its emanation point (Figs. 5 and 10); the propagation vergence of the wing is to the southwest intruding at an angle of ca. 30° (Fig. 10c). This angle of intrusion was probably higher in the moment of the intrusion and was flattened as a result of compaction. As noted by Huuse *et al*. (2004) the geometry and scale of this wing is similar to wings mapped from interpretation of seismic data, frequently occurring along the margins of saucer-shaped intrusions (Polteau *et al*. 2008; Jackson *et al*. 2011; Hurst & Vigorito 2017).

Intrusions in the upper intrusive network display a greater range of geometry, size and internal structures than those present in the lower intrusive interval. Dykes crosscut bedding in the host strata at low and high angles, and have a large range of apertures (0.01 to 12 m) (Figs.11 and 12). The emplacement of these intrusions disrupted the host strata creating “jack up” of the overlying mudstone as the sills dilated (Fig. 11a). Individual dykes may include several geometric styles ranging from sheet-like with planar margins to highly irregular, bulbous and curved margins

(Fig. 11; cf. Surlyk *et al.* 2007). Internal structures include banding and laminae, particularly adjacent to margins and in the central areas of dykes. Alignment of elongate clasts, including fragments of the host mudstone, along with aligned oxidation inside intrusions define banding. When adjacent to brecciated intervals, intrusions are commonly enriched in angular and rounded clasts of host mudstone that form conglomeratic pockets (0.05 to 0.3 m thick) aligned sub-parallel and oblique to the intrusion margins. Aligned clasts in the upper intrusive interval are useful to infer the flow direction of fluidised sand. Intrusive chimneys commonly occur in the junction where large sills are connected by thinner dykes on top and indicate the upward flow of the sand and clasts.

In terms of relative thickness, the upper intrusive interval behaves similarly to the lower intrusive network, with intrusion thickness decreasing upward away from its parent units (Fig. 12). Intrusive sandstone in the uppermost part of the upper intrusive interval is less common and thinner (0.1 to 0.5 m aperture) with a predominance of dykes. In the east portion of the study area an erosional unconformity cuts the top of the upper intrusive interval followed by the deposition of sandy conglomerate and sandstone of the Tumey Sandstone Lentil (Figs. 5 and 15). A conglomerate composed of reworked breccia clasts of biosiliceous mudstone and sandstone is frequently present along the base of the unconformity (Fig. 15) constraining the formation of the TGIC to the limit between the upper Eocene and lower Oligocene.

Injection Breccia

Large scale breccia zones occur almost exclusively in the upper intrusive interval, especially in the biosiliceous mudstone strata. These zones have irregular and discontinuous sub-horizontal distribution in the upper intrusive interval, reaching up to 80 m thick and extending laterally up to 1.3 km (Fig. 5). No evidence of depositional processes is associated with the injection breccia, and its formation is interpreted to be the result of intense hydraulic fracturing of the host mudrocks with simultaneous sand injection. The breccias are largely monomitic, comprising clasts of biosiliceous mudrocks with a broad size-range (>1 mm up to 3m diameter) and shapes (angular to rounded), within a sandy matrix (Figs. 13 and 14). They present a highly heterogeneous geometry intensely disrupting the original bedding of the host mudstones.

The sandstone forms a complex network of irregular dykes and sills between mudstone clasts, hence termed an injection breccia, similar to the mudstone clast breccia, facies B4 of Duranti and Hurst (2004). The injection breccias comprise different facies, with angular and rounded mudstone clasts that were incorporated into a matrix of structureless, ungraded sandstones (Figs. 13b). A variety of textures and structures occur, ranging from a chaotic fabric where the clasts show a random disposition, to an orientated organization with the alignment of clasts marking the flow direction which is mostly sub-parallel to the margins. Clast geometry ranges from predominantly very angular and platy fragments to rounded, with a matrix of medium-grained lithic sandstone very similar to the grain size and composition of the turbiditic sandstone, supporting their genetic relationship.

The range of facies in the breccia and the crosscutting relationships between them reflect different pulses of flow during sand emplacement. Three main broad injection breccia facies were defined on the basis of structures and textures:

(1) **Blocky injection breccia facies**: mostly comprise clast-supported breccias with high content of tightly packed angular clasts of mudstone (>75% clasts), in a sandstone matrix, with little or no evidence of significant clast rotation and transportation (Fig. 14a). This breccia facies is interpreted to be formed *in situ* by intense hydraulic fracturing of the host strata and sand injection into the propagating fracture network, thus giving rise to thin sandstone intrusions (1-30 cm thick) that separate adjacent clasts of host strata commonly in jigsaw geometry (Fig. 13b).

(2) **Dispersive injection breccia facies:** this facies comprises mostly matrix-supported injection breccia with minor clast-supported injection breccia, with a variable quantity of mudstone clasts of different size and shape (Figs. 13 and 14). Tightly and loosely packed clasts occur, showing angular and rounded external geometry (Fig. 13d). Textural and spatial relationships between clasts vary and record a process of differential fragmentation, along with clast rotation, transportation and

erosion. It is interpreted that the varied intensity of hydraulic fracturing of host strata resulted in irregular clast size distribution within the fluidised sand, producing a broad range of clasts sizes (Fig. 14b). Occurrence of imbricated platy and elongated clasts indicate the approximate flow direction of the injection, specifically in tabular sills and dykes (5-15 cm thick) where the injection flow is restricted to the intrusion margins.

(3) **Sandstone intrusion facies**: essentially composed of sandstone, this facies is identical to the typical sandstone fill of sills and dykes of the intrusive complex but, in the context of the breccia, the sandstone was emplaced into irregular conduits that cut the blocky and dispersive breccias (Fig. 14a, c and e) as a last stage of the sand emplacement. Mudstone clasts from adjacent host units commonly concentrate along the margins or in the central portion of the intrusions (Fig. 13b).

Interpretation of injection breccia

Examples of injection breccia occurs in other outcrops (Hurst *et al*. 2006; Briedis *et al*. 2007; Surlyk *et al.* 2007) and subsurface examples (Dixon *et al.* 1995; Duranti *et al.* 2002; Duranti & Hurst 2004; De Boer *et al.* 2007; Hurst & Vigorito 2017). TGIC injection breccia is however, substantially thicker, and is restricted to the shallowest part of the intrusive complex. Although the theoretical conditions for the initiation of brittle failure are well known, it is problematic to constrain these conditions in poorly-consolidated strata in the very shallow subsurface where sand injection is most often interpreted to occur (Hurst & Cartwright 2007; Hurst *et al*. 2011). Formation of an injection breccia, in which a wide range of fracture geometry and orientation occurs, requires only that:

$$P_f > \sigma_3 + T \qquad (1)$$

and,

$$P_f > \sigma_n \qquad (2)$$

where, P_f = pore fluid pressure, σ_3 = the minimum principle stress, σ_n = resolved normal stress and T = the tensile stress of the host strata (Vigorito & Hurst 2010).

For the injection breccia to form, conditions (1) and (2) co-existed, and following an initial period of intense hydraulic fracturing sustained flow of fluidised sand occurred into localised dilated fractures (Hurst *et al*. 2011).

Injection breccia occurs in the upper intrusive unit, both above and adjacent to thick parent sandstone, and shallower, where it forms in biosiliceous mudstone and is regionally extensive. This contrasts with the PGIC, where breccia is typically associated with deeper sections of the injection complex, and specifically with the sill zone and the intense hydraulic fracturing of host strata (Vigorito & Hurst 2010; Hurst *et al*. 2011). Breccia in the PGIC is neither as thick nor as laterally extensive as in TGIC. A possible analogue of breccia formation immediately below a palaeo-seafloor described from the Santa Cruz Mudstone (Miocene) (Hurst *et al*. 2006; fig. 9a) is texturally similar to the TGIC breccia, although less thick (<4m), laterally discontinuous and much less extensively exposed.

Most clasts formed by hydraulic fracturing of the host biosiliceous mudrocks and their detachment from intrusion margins into fluidised sand. Rounded clasts generated by clast abrasion in the fluidised sand-flow record exposure to persistent turbulent flow. Where clasts with angular and abraded margins co-occur is evidence of sand injection simultaneously propping open some fractures while other fractures, and other parts of the same fracture, dilated, closed and re-dilated in response to variations in pore fluid pressure. Prolonged entrained flow causes differential rounding of clasts.

Structural analysis

Intrusion geometry of sand injectites is influenced by the mechanical properties of host strata, the overpressure conditions of depositional parent units, the stress field at the time of emplacement, and the presence of any pre-existing structures (Cosgrove 2001; Jolly & Lonergan 2002). The structural patterns of sandstone intrusions and injection-related fractures of host units were examined throughout the Tumey Hill area, although most of the outcrop belongs to the upper portion of the TGIC (upper intrusive interval) thus limiting quantitative analysis.

Restoration of tectonic dip to depositional configuration reveals a structural control of the TGIC intrusions and fractures in the host mudstone which resulted a preferential orientation NW-SE (Fig. 16a). As expected, bedding attitude controls sill geometry in a sub-horizontal orientation. Fractures in the host strata and dykes have similar orientations with NW-SE strikes mainly dipping to NE and subordinately to SW (Fig. 16a). Analysis of the scattering diagram of sandstone sills and dykes (Fig. 16b) identified two main striking directions controlling the intrusions. A SE-striking set (strikes ranging from 60° to 180°) with dykes dipping at high angles (50°-90°) to SW (black dashed square); and a NW-trending set (strikes 240° to 360°) with dykes dipping with lower angles (30° - 70°) to NE which form the main intrusive systems of the complex. The NW-SE striking dykes, mainly dipping to NE with mean vector 320/40, is consistent with the strike of the main fracture system present in the host strata (NW-SE striking fractures plunging to NE with mean vector 325/42).

When plotted, the attitude of the intrusions was highly variable, however a girdle distribution is recognizable from the polar plot for the planes (Fig.16d), which shows that intrusions strike predominantly NW–SE, forming two main plane sets dipping mainly to NE and to SW. This structural configuration is characteristic of an asymmetric saucer-shaped intrusion geometry, with a few small wings plunging at high angles (40-60°) to S-SW, with vergence to N-NE, and larger and far more numerous wings with axes plunging at lower angles (20°- 40°) to NE and verging mainly to SW. This was observed at the Half Dome outcrop (Fig. 10).

Paleo-stress analysis

The orientation data from the intrusive bodies provided an opportunity to define palaeo-stress fields during their emplacement (Boehm & Moore 2002) as they are formed by opening fractures that propagate as a tensile crack in a plane normal to the direction of the least compressive stress (Delaney *et al*. 1986). The emplacement of sheet-like intrusions (igneous or clastic) is commonly associated with Mode I fracturing (Anderson 1951) in which dilation is perpendicular to the fracture plane, so structural analysis of intrusions is crucial when constraining *in situ* stress at the time of emplacement (Stephens *et al.* 2018). For an intrusion to propagate, overpressure in depositional sandstone (parent units) must exceed the minimum principal stress (σ3) plus the tensile strength (T) of the host rock (Cosgrove 2001). The minimum compressive stress (σ3) is commonly perpendicular to the extension fracture walls (Delaney *et al.* 1986), and local deflections of the intrusion attitude are inferred to represent local rotation of the stress axes or local heterogeneities of the host rocks. This model implies that intrusions can propagate locally out of the regional σ1– σ2 plane, via Mode I failure of intact strata, or through Mode I dilation of pre-existing structures, producing intrusions that display variable dilation vectors along a single intrusion (Stephens *et al.* 2018).

A mechanical model for the emplacement of the TGIC using field-based measurements of intrusion and fracture attitude was derived from the relative stress field axes during sand injection (Fig. 17). Based on the stereoplot of poles of the sandstone intrusions (dykes) and fractures of host strata, the main stress fields of the injection complex were defined (Fig. 17a). By determining the orientation of the sheet-like intrusion (dyke or sill) and its dilation direction the relative minimum compressive stress (σ3) of the system was defined. As there was no evidence that the intrusions were injected into pre-existing fractures, the majority of the intrusions should reflect the orientation of the palaeo-stress field at the time of their emplacement.

Using a similar method to that used by Boehm & Moore (2002), the overall strike and dilatational orientation of the intrusive bodies was analysed, which in turn defined an approximate spatial orientation of the regional strain related to the intrusive process. Orientations are represented by eigenvalues and eigenvectors for the distribution of all intrusions (Fig. 17a). The largest eigenvector/eigenvalue (e1) of the dykes (Fig. 17a) plunges 45° to SW, indicating maximum dilation perpendicular to the NE-dipping dyke walls. The intermediate eigenvector/eigenvalue plunges at a low angle NW (22° to 332°), and corresponds approximately to the sub-horizontal orientation of the bedding and is considered to be the rotational axis of the strain ellipsoid (σ2). The minimum eigenvector/eigenvalue indicates the least dilatational strain, and plunges 38° to 080° (ESE).

The NW-striking dikes plunging to NE (Fig. 17) suggest a minimum principal stress (σ3) that plunges obliquely at 45° to the SW, and the contemporaneous sills indicate a minimum principal stress with a sub vertical orientation (Fig. 17b). This configuration is explained by the dykes and sills intruding into the overburden perpendicular to their relative minimum principal stress, with weaker sediment cohesion subparallel to bedding (Boehm & Moore 2002). As the lower intrusive interval is sill-dominated, the presence of a predominantly sub vertical minimum principal stress (σ3) was inferred (Fig. 17b). The overall structural configuration of the complex constrains the maximum principal stress axis direction to be NE-SW plunging ca. 38° indicating a predominant principal compressive direction ENE-WSW with the minimum principal stress axis (σ3) plunging around 40° to SWS (Fig. 17a).

Discussion

The only other known exposure of a regionally developed giant sand injection complex is the neighbouring, older Panoche Giant Injection Complex (PGIC, Vigorito *et al*. 2008; Vigorito & Hurst 2010), therefore the characterization of the TGIC as an analogue is a significant increase in knowledge. In that context, and given the similar tectono-sedimentary setting within the Great Valley Group (Ingersoll 1982), it is noteworthy that the TGIC and PGIC are so different. Several smaller outcrops that expose parts of sand injection complexes with similar intrusion geometry to each other have been described (Parize & Friès, 2003; Parize *et al.* 2007; Surlyk *et al.* 2007; Scott *et al*. 2009; Kane 2010; Cobain *et al*. 2015; Ravier *et al.* 2015). Despite their apparent similarity, these papers draw different conclusions regarding direction of dyke propagation and the prevailing flow regime during sand fluidisation. In both TGIC and PGIC, excellent vertical and lateral exposure allow more confident and holistic interpretation of characteristics and processes (Vigorito &Hurst 2010; Hurst *et al*. 2011; Hurst & Vigorito 2017).

Geometry and architectural framework

Two distinctive characteristics of TGIC architecture are that depositional sandstone is present throughout most of the injection complex (Figs. 5 and 18a) and that the underlying strata (pre-Kreyenhagen) did not provide a significant volume of fluid during sand fluidisation. Evidence of sand fluidisation is present in all depositional sandstones and all parent sandstone intrusions. In the PGIC, only the Dosados Sandstone parent has contributed significant sand volume (Vigorito & Hurst 2010; Hurst et al. 2017). Where shallower depositional sandstone occurs, sandstone intrusions disrupt them but with insignificant evidence of fluidisation. The absence of an underlying aquifer to source fluids and fluid overpressure in the TGIC implies laterally offset aquifer supply. The difference with respect to aquifer gives TGIC an immediate relevance to subsurface sand injection complexes that lack large underlying aquifers.

Sandstone intrusion geometry and scale in TGIC is similar to those in other well-exposed sand injection complexes (Surlyk *et al*. 2007; Vigorito *et al*. 2008; Vigorito & Hurst 2010; Scott *et al*., 2013) and those in subsurface (Duranti & Hurst 2004; Huuse *et al*. 2004; Jackson 2007) with often-dense networks of dykes, sills and composite intrusions forming saucer-shaped and wing-like intrusions (Fig. 18). In TGIC, proximity and size of sandstone parent units controls the size and abundance of intrusions, and forms a vertical section of approximately 450m, where all parent units are intensely fluidised (Fig. 18a). The intrusions are highly interconnected (Figs. 7, 10, & 11) with sills and saucers forming km-scale horizontally linked units and dykes creating vertical conduits. In general, the intensity of intrusions is similar to the PGIC sill zone (Vigorito & Hurst 2010). Intrusion thickness decreases upward in both the lower and upper intrusive intervals (Fig. 12), trends that correspond to vertical depletion of pore-fluid pressure upward during sand injection. Distribution of similarly sized parent units throughout the TGIC, with the exception the uppermost channel (Fig. 5), is distinctly different from that observed in the PGIC or elsewhere. In subsurface injection complexes, steep low aperture dykes are rarely resolved (Skjaerpe *et al*. 2018; Satur *et al*. *this volume*) and dependent on depth and seismic frequency sills and saucers below ~5 to 10 m are also not resolved and most dykes steeper than 45° to bedding are undetected (Huuse *et al*. 2007; Grippa *et al*. 2019).

A pattern of “sills shallow, dykes deep” (Jolly & Lonergan 2002) is absent in the TGIC and PGIC. In the very shallow section of the PGIC rare sills occur (Vétel & Cartwright 2010; Vigorito & Hurst 2010). Multi-layered sills in TGIC (Figs. 7a & 18a) occur mostly in the lower intrusive interval, a similar spatial arrangement to the PGIC where multi-layered sills are associated with the shallow part of the sill zone (Vigorito *et al*. 2008) (Figs. 18b). Saucer-shaped sills and wings in the TGIC predominate in the upper intrusive interval, and unlike in the PGIC, where saucers and wings typically combine to form large composite intrusions (Vigorito & Hurst 2010; Grippa *et al*. 2019), at Tumey Hill they are smaller and less frequently composite. An exception to this is the large composite wing at the Half Dome outcrop (Figs. 10 & 11), which occurs near the base of the upper intrusive interval (Fig. 18). Only recently was the composite character of subsurface wings resolved (Satur *et al*., this volume).

In common with large saucers and wings in the PGIC, the Half Dome wing has direct linkage to a parent unit (Figs. 10 & 18a). In the PGIC, large saucers and wings tend to be the shallowest large intrusions in the sill zone (Hurst & Vigorito 2017; Grippa *et al*. 2019) (Fig. 18b). Subsurface relationships between parent units, sills, saucers and wings are extremely difficult to constrain, indeed interpretation of surface data is typically instrumental in supporting subsurface interpretations (Briedis *et al*. 2007; Hurst *et al*. 2016; Satur *et al. this volume*). Common identification of saucers and wings on seismic data (Huuse *et al*. 2005; Jackson *et al*. 2011) may reflect their occurrence in the shallower parts of injection complexes relative to sills and parent units. Although the overall TGIC architecture contrasts with that of PGIC, individual intrusion geometry is similar and the spatial arrangement of the sill, saucer and wing intrusions has similar architecture. It is likely that the “shallow sill” architecture (Jolly & Lonergan 2002) is somewhat compromised by the limited extent of the outcrop on which it is based (Fig. 2).

Host strata characteristics may influence the geometry and architecture of sandstone intrusions, but to date it is unclear which characteristics are most influential. TGIC's lower and upper intrusive intervals are rich in clay minerals and opaline silica, respectively. Today, the clay mineral rich mudstone is laminated, compacted and poorly to moderately consolidated, whereas the bio siliceous mudstone is largely structureless, low density and cemented. At the time of sand injection they were probably similarly poorly consolidated although with a laminar microstructure in the former, and granular texture in the latter. Multi-layer sills in the clay mineral rich lower intrusive complex are overall discordant to bedding, but crudely bedding- or lamination-parallel (Fig. 7a, b) suggesting that exploitation of weakness along lamination or bedding probably focused early propagation of hydraulic fractures. However, the combination of continued hydraulic fracturing and erosion by turbulent flow of fluidised sand dominated (Vigorito and Hurst, 2010; Hurst et al., 2011) and created the prevailing discordance (Figs 7, 10, 13 & 14). Discordant margins are pervasive and diagnostic in sand injection complexes, and is a much-used criteria applied to subsurface differentiation of depositional vs injected facies (Dixon *et al*. 1995; Duranti *et al*. 2002; Hurst et al. 2011).

Coincidence of the NW-SE strike of dykes with the main fracture system (Fig. 16) records a structural control during sand injection. If similar relationships exist in the subsurface, sandstone intrusions within larger sand injection complexes, provide insight into prevailing stress at the time of intrusion and whether that coincides with tectonism or the basin framework. In the PGIC, Smyers & Peterson (1971) recorded a concordant relationship between orientation of dykes (the upper dyke zone of Vigorito & Hurst 2010) and the prevailing tectonic stress, confirmed by a more complete analysis of sandstone intrusions from the entire PGIC (Vigorito & Hurst 2010). Unfortunately, a lack of similar well-exposed regionally developed outcrop of sand injection complexes limits further comparison. In the much less extensive exposure of the Vocontian Basin (SE France), Monnier et al. (2015) reached similar conclusions. Recognising relationships between tectonic stress and the orientation of intrusions is salient in subsurface analysis when evaluating the distribution and orientation of sub-seismic scale intrusions (Skjaerpe et al. 2018).

Geological Controls and Trigger Mechanisms of TGIC

Formation of Giant Injection Complexes requires development of regional overpressure in the very shallow crust in which poorly consolidated depositional units are located close to or within the zones of intense hydraulic fracture. Previously the only outcrop where this has been described on a regional scale is the nearby Panoche Giant Injection Complex (PGIC, Vigorito & Hurst 2010). Many triggers may cause sand injection but diagnostic evidence is sparse (Hurst *et al*. 2011). Much of the conjecture is associated with the generation of pore-fluid overpressure and its focus in limited areas of large sedimentary basins. In that context, the TGIC has constraints helpful in this analysis, as regionally the structural setting and evolution of the area is the subject of much independent research, and locally the excellent outcrop allows detailed evaluation of relationships between intrusions and palaeo-stress.

The predominant NW-SE strike of the sandstone intrusions and the related fracture system of the TGIC (Figs 16 and 17) is sub parallel to the NW-SE oriented axis of the San Joaquin Basin at the time of emplacement of the injection complex (Fig. 19). This observation opens the possibility of relating the emplacement of the TGIC with the tectonic evolution and palaeo-architecture of the basin. Contractional tectonics associated with the subduction of the Farallon plate mainly controlled the structural architecture and deposition of the GVG. Along the western edge of the basin evidence for extensional tectonics is recorded by broad subsidence (Platt 1993; Unruh *et al.* 2007) and normal faulting along with the uplift of the Franciscan Complex (Harms *et al*. 1992; Unruh *et al*. 2007). Exhumation of the Franciscan Complex and the adjacent Great Valley forearc evolution, suggests that the forearc basin was characterized by an extensional regime with active subsidence and sedimentation until late Eocene (cf. Unruh *et al*. 2007, fig. 12). From the late Cretaceous to late Eocene, extensive NE-dipping low angle normal faults in the western part of the GVG formed associated with the uplift of the Franciscan Complex (Dumitru 1989; Krueger & Jones 1989; Unruh *et* *al.* 2007). Location of the TGIC on the western margin of the basin meant that the related extensional and/or contractional deformation had a greater influence than may be expected elsewhere in the basin. Beginning early in the Tertiary, and continuing episodically throughout, the attenuated forearc crust was uplifted, tilted and folded by deep-seated west-dipping thrust faults (Unruh *et al*., 2004), and contractional deformation cannot be disregarded as a potential mechanism to drive stress within the basin during formation of the injection complex.

Lack of evidence of a source of fluid in the underlying Lodo and Domengine formations means that lateral ingress of pore fluid is most likely the source of the overpressure that led to formation of the TGIC. Lateral pressure transfer occurs because of depositional tilting and subsequent up-dip migration of fluids into sandstones closer to a basin margin (Osborne & Swarbrick 1997; Yardley & Swarbrick 2000; Flemings *et al.* 2002). TGIC's location within a large submarine system within which numerous sandstone-rich channels and channel complexes occur, suggests the identity of the main conduit for lateral pressure transfer (Fig. 19c). All sandstone intrusions in TGIC are physically connected to depositional sandstone units (summarised in Figs 3, 5, and 18A), which were the sources of sand (as confirmed by light and heavy mineralogy), and fluid to the injection complex. The TGIC slope setting is expected to have an axially fed hydraulic structure probably linked to the palaeo-Sierra Nevadan mountains (Fig. 19b). This contrasts markedly with the PGIC (Fig. 18b), which is underlain by a very thick (>10km) aquifer that is the main source of fluid and pressure, to form the PGIC (Vigorito & Hurst 2010). Provenance of known subsurface examples with similar relationships between injection complexes and large underlying aquifers (Huuse *et al*. 2005; Satur & Hurst 2007; Morton *et al*. 2014; Hurst *et al*. 2016) also have distinct mineral provenance associated with sand derivation from the shallow part of the underlying aquifer (Morton *et al*. 2014; Hurst *et al*. 2017). It is clear that creation of a sustained rapid ingress of pore-fluid sufficient to create regional hydraulic fracturing during shallow burial required exceptional conditions.

Based on coincidence of the predominant NW-SE orientation of intrusions with the regional stress field and architectural framework of the San Joaquin Basin during the Eocene, we infer that hydraulic fracturing of host strata and sand emplacement are associated with regional tectonic stress in the basin (Fig. 19a, c). If sand injection was uninfluenced by tectonic stress, an alternative control could be gravitationally induced stresses associated with slope instability. Because the TGIC is emplaced into a slope succession on an active margin, it is reasonable that periodic intense seismicity would induce gravitational collapse of the slope. This is recorded in the underlying Domengine Formation ca. 20 Km south of the TGIC as the New Idria mass-transport deposit (Sharman et al., 2017). The New Idria MTD is associated with soft-sediment folds and reverse faults that record transport toward the west to southwest that were controlled by the gravitational instability and eventual collapse of the shelf. Sharman et al. (2017) suggest that (1) high sedimentation rates, (2) loading of poorly compacted, mechanically weak, fine-grained units overlain by denser units, and (3) seismicity, were the main drivers of mass failure. Slope turbidites and mudstones in the Kreyenhagen Shale, could have undergone similar gravitational instability to those in the underlain estuarine and deltaic Domengine formation. Most of the dykes and the winglike intrusion of the TGIC strike NW-SE and dip to NE, implying a predominant injection emplacement toward southwest. This configuration is coincident with the main folds and reverse faults present in the New Idria MTD, attributed to structural control of the NW-SE strike of the paleo-shelf and slope. Sand injection and slope failure have coincident NW-SE structural trends and record different deformation processes along the same margin.

Although we have no evidence of gravity failure in the Domengine Formation underlying the study area, one cannot discount that gravity-driven instability influenced sand injection in the Kreyenhagen formation. However, the balance of evidences suggests that formation of the TGIC was a consequence of burial and compaction of channelized turbiditic sandstone sealed within low-permeability mudstone, combine with focused lateral fluid migration (Osbourne & Swarbrick, 1997) into the sandstone that caused overpressure. This occurred during a period of extensional tectonics that triggered and focused hydraulic fracturing of the host strata and caused sand injection (Fig. 19).

TGIC as a subsurface analogue

Subsurface analogues of sandstone intrusions are important in petroleum (and other fluid) systems in the context of understanding reservoir geometry and architecture, estimating aquifer support (Briedis *et al*. 2007; Schwab *et al.* 2015) and when identifying fluid migration conduits (Jenkins 1930; Hurst *et al*. 2003a). Other applications include the identification of the geologically instantaneous sand extrudites (Hurst *et al*. 2006) and elucidating overpressure development and seal integrity (Cartwright *et al*. 2007). As an analogue for subsurface analysis, the TGIC is exceptional because of its large area and high quality exposure, and because the reservoir architecture is significantly different than that present in the PGIC, the only other regionally developed giant sand injection complex (Vigorito & Hurst 2010; Hurst *et al*. 2011).

Arguably, the most distinctive characteristics of the TGIC when compared with the PGIC are that depositional sandstone is present throughout most of the section (Fig. 18a) and the importance of the laterally offset aquifer (Fig. 19). The latter gives TGIC an immediate relevance to subsurface basin margin development of injection complexes where sedimentary units thin, large underlying aquifers are absent, or underlying strata constitute very low porosity sedimentary or crystalline basement. “Injectite” oilfields in basin marginal locations are present along the eastern and western margins of the Viking Graben where major aquifers are largely absent below the injection complexes or offset laterally by 10’s of kilometres (Dixon *et al.*, 1995; Mangerud *et al*. 1999; Bergslien 2002; Briedis *et al*. 2007; McKie *et al*. 2015). Because of the architecture of depositional sandstone in TGIC, sand fluidisation and injection affected all depositional sandstone and hence, supra-lithostatic pore-fluid pressure was pervasive, implying that most of the TGIC formed within the sill zone (*sensu* Vigorito & Hurst 2010). Clear relationships exist between large depositional parent units and the largest intrusions, for example, the Half Dome wing (Figs. 10 & 11). In the TGIC, depositional units feed directly into sandstone intrusions and have similar composition (Fig. 18a). In the PGIC, sandstone intrusions connect to a single depositional parent unit, the Dosados Sandstone (Vigorito &

Hurst 2010; Hurst et al. 2017) (Fig. 18b). In subsurface settings where depositional sandstone has a high N/G throughout an injection complex the TGIC is a highly relevant analogue (Fig. 18).

Gradational changes in composition typify the PGIC host strata (Moreno Formation, Payne 1951; Vigorito & Hurst 2010) and are similar to many subsurface mudstone hosts of sandstone intrusions. At the time of injection, host strata in TGIC had contrasting gross porosity structures, ranging from granular in a biosiliceous ooze and laminated in the clay-rich mudstone. The granular ooze would have dissipated pore-fluid pressure more rapidly than the laminar mudstone and appears to have had induced brecciation (Figs. 13 and 14). Injection breccia is less well developed in clay-rich host strata in both the TGIC and PGIC.

Sandstone intrusions, including breccia, cross-cut hundreds of metres of mudstone-dominated Kreyenhagen Shale and form highly permeable conduits for fluid flow through an otherwise low permeability succession (c.f. Jenkins 1930; Hurst *et al*. 2003a; Hurst *et al*. 2003b; Huuse *et al.* 2005; Briedis *et al*. 2007; De Boer *et al.* 2007). In the subsurface, sand injection complexes preserve intrusions with wing-like and saucer-shaped geometry that are typical targets of exploration and field development wells in (Duranti et al. 2002; Huuse et al. 2003; DeBoer et al. 2007; Szarawarska et al. 2010, Satur *et al*. this volume). Outcrop of wing-like intrusion are similar those identified in subsurface (Huuse et al. 2007; Grippa et al., 2019). The TGIC wing extent laterally for up to 600m emanating from the parent turbiditic channel and crosscutting the host mudstone by at least100m. Similar geometry and scale wings occur in the North Sea basin in the Alba and Volund Field (Duranti and Hurst, 2004; Huuse et al., 2004; Satur et al., this volume) (Fig. 18). These and other similar characteristics of sandstone intrusions in the subsurface demonstrate the relevance of TGIC as an outcrop analogue with fundamentally different architecture and origin to the PGIC (Vigorito and Hurst, 2010).

Conclusion

Turbiditic sandstone that occurs through most of the TGIC section acted as parent units for sandstone intrusions. The intrusive network sourced by these parent units presents a complex architectural organization with varied intrusive bodies geometries and sizes. Sills complex, including multi-layer sills prevail in the lower intrusive interval whereas the upper intrusive interval is characterised by asymmetric saucer and wing-like intrusions. This trend is similar to that observed in other giant injection complexes. Injection breccia is common adjacent to large depositional sandstones and intrusions emanating from them, and forms a thick (up to ~50m) and laterally extensive unit in the upper intrusive interval. Breccia forms significant reservoir volume, and where laterally extensive gives hydraulic continuity across the shallow section of the injection complex. Large intrusions are associated with the largest depositional parent units, which because present throughout the TGIC create a highly connected and volumetrically significant reservoir network.

Lower and upper intrusive intervals do not coincide with variation from mudrocks enriched in clay minerals to a bio siliceous mineralogy. Therefore the host mudrock mineralogy and resultant internal structures do not exert a major control on the geometry of sandstone intrusions. Mudstone mineralogy does not correlate with the occurrence of the entire injection breccia zones although bio siliceous mudstone is the host for the laterally extensive breccia zone. Lamination is evident in clay rich mudstone, which hosts sills, but it does not control their external geometry.

Overpressure was generated laterally from along the axis of coarse-grained deposition, with no evidence of an underlying aquifer active at the time of sand injection. Coincident NW-SE orientation of wing like intrusions with the dominant structural framework of the basin indicates that sand injection occurred during a period of extension possibly controlled by tectonic or gravity driven stress. A late Eocene early Oligocene erosional unconformity cuts the top of the TGIC truncating high angle dykes and the host biosiliceous mudstone with, in places, more than 20 m erosion, constraining the injection event to the Late Eocene.

TGIC has seismic-scale outcrop ideal for supporting subsurface reservoir modelling. It is a significantly different giant injection complex than the previously-described PGIC, with contrasting relationships between parent units and intrusions, aquifer location, abundance and distribution of injection breccia, while retaining a record of similar processes, intrusion geometry and internal structures.

Acknowledgments

The authors gratefully acknowledge support from Shell Brazil and CNPq through the "BG05: UoA-UFRGS-SWB Sedimentary Systems" project at UFRGS and UoA and the strategic importance of the support given by ANP through the R&D levy regulation. We also wish to thank the support from the Sand Injection Research Group (SIRG) and the researchers who collaborated during fieldwork. We also wish to thank the support and help of the Bureau of Land Management (CA) providing guidance and legal access to the study area.

References

Anderson, F.M. 1905. A Stratigraphic Study in the Mount Diablo Range of California. *Proceedings of the California Academy of Sciences*, third series. *Geology*, vol.2, no. 2, p. 156-252.

Anderson, R. & Pack, R., 1915. Geology and Oil Resources of the West Border of the San Joaquin Valley North of Coaling, California. *United States Geological Survey Bulletin,* 603, 220 p.

Anderson, E.M. 1951. *The Dynamics of Faulting and Dyke Formation with Application to Britain 2nd ed.*, 206 pp., Oliver and Boyd, Edinburgh.

Atwater, T. 1970. Implications of Plate Tectonics for the Cenozoic Tectonic Evolution of Western North America. *GSA Bulletin*, **81**, 3513–3536.

Atwater, T. & Stock, J. 1998. Pacific-north america plate tectonics of the neogene southwestern united states: An update. *International Geology Review*, **40**, 375–402, https://doi.org/10.1080/00206819809465216

Bartow, J. & Nilsen, T. 1990. Review of the Great Valley sequence, eastern Diablo Renge and northern San Joaquin Valley, Central Calofornia. *U.S. Geological Survey Professional Paper*, p. 25.

Bartow, J.A. 1991. Cenozoic evolution of the San Joaquin Valley, California. *U.S. Geological Survey Professional Paper*, p. 1–40.

Bartow, J.A. 1996. Geologic map of the west border of the San Joaquin Valley in the Panoche Creek–Cantua Creek area, Fresno and San Benito counties, California. *Miscellaneous Investigations Series—US Geological Survey Map*, I-2430.

Bergslien, D. 2002. Balder and Jotun - two sides of the same coin? A comparison of two Tertiary oil fields in the Norwegian North Sea. *Petroleum Geoscience*, v. 8, p. 349–363, https://doi.org/10.1144/petgeo.8.4.349.

Boehm, A. & Moore, J.C. 2002. Fluidized sandstone intrusions as an indicator of Paleostress orientation, Santa Cruz, California. *Geofluids*, **2**, 147–161, https://doi.org/10.1046/j.1468-8123.2002.00026.x

Briedis, N.A., Bergslien, D., Hjellbakk, A., Hill, R.E. & Moir, G.J. 2007. Recognition Criteria, Significance to Field Performance, and Reservoir Modeling of Sand Injections in the Balder Field, North Sea. *In*: Hurst, A., Cartwright, J. (Eds.), *Sand injectites: Implications for Hydrocarbon Exploration and Production*. American

Association of Petroleum Geologists Memoir, Tulsa, pp. 91–102.

Braccini, E., de Boer, W., Hurst, A., Huuse, M., Vigorito, M. & Templeton, G. 2008. Sand Injectites. *Oilfield Review*, **20**, 34–49.

Cartwright, J., Huuse, M. & Aplin, A. 2007. Seal bypass systems. *AAPG Bulletin*, v. 91, p. 1141–1166, doi: 10.1306/04090705181

Cartwright, J. 2010. Regionally extensive emplacement of sandstone intrusions: A brief review. *Basin Research*, 22, 502–516, https://doi.org/10.1111/j.1365-2117.2009.00455.x

Cobain, S.L., Peakall, J. & Hodgson, D.M. 2015. Indicators of propagation direction and relative depth in clastic injectites: Implications for laminar versus turbulent flow processes. *Bulletin of the Geological Society of America*, 127, 1816–1830, https://doi.org/10.1130/B31209.1.

Cobain, S.L., Hodgson, D.M., Peakall, J. & Shiers, M.N. 2017. An integrated model of clastic injectites and basin floor lobe complexes: Implications for stratigraphic trap plays. *Basin Research*, https://doi.org/10.1111/bre.12229.

Cosgrove, J.W. 2001. Hydraulic fracturing during the formation and deformation of a basin: A factor in the dewatering of low-permeability sediments. *American Association of Petroleum Geologists,* **85**, 737–748.

Davies, R.J., Huuse, M., Hirst, P., Cartwright, J. & Yang, Y. 2006. Giant clastic intrusions primed by silica diagenesis. *Geology*, **34**, 917–920, https://doi.org/10.1130/G22937A.1

De Boer, W., Rawlinson, P.B. & Hurst, A. 2007. Successful Exploration of a Sand Injectite Complex: Hamsun Prospect, Norway Block 24/9. *In*: Hurst, A., Cartwright, J. (Eds.), *Sand Injectites: Implications for Hydrocarbon Exploration and Production*. American Association of Petroleum Geologists Memoir, Tulsa, pp. 65–68.

Delaney, P.T., Pollard, D.D., Ziony, J.I. & McKee, E.H. 1986. Field relations between dikes and joints: Emplacement processes and paleostress analysis. *Journal of Geophysical Research*, **v. 91**, p. 4920, doi: 10.1029/JB091iB05p04920

Dickinson, W.R. & Seely, D.R. 1979. Structure and Stratigraphy of Forearc Regions. *AAPG Bulletin*, 63, 2–31, https://doi.org/10.1306/C1EA55AD-16C9-11D7-8645000102C1865D.

Dickinson, W.R. 1981. Plate tectonics and the continental margin of California. *In:* Ernst, W. G. (ed) *The geotectonic development of California*. Englewood Cliffs, Prentice-Hall, pp. 1–28.

Dickinson, W.R. 2002, Reappraisal of hypothetical Franciscan thrust wedging at Coalinga: Implications for tectonic relations along the Great Valley flank of the California Coast Ranges. *Tectonics*, **v. 21**, no. 5, p. 1039, doi: 10.1029/2001TC001315

Dixon, R.J., Schofield, K., Anderton, R., Reynolds, A.D., Alexander, R.W.S., Williams, M.C. & Davies, K.G. 1995. *Sandstone diapirism and clastic intrusion in the Tertiary submarine fans of the Bruce-Beryl Embayment, Quadrant 9, UKCS*. Geological Society, London, Special Publications, **v. 94**, p. 77–94.

Dumitru, T.A., 1989. Constraints on uplift in the Franciscan Subduction Complex from apatite fission track analysis. *Tectonics*, **v. 8**, p. 197–220, doi: 10.1029/TC008i002p00197

Duranti, D., Hurst, A., Bell, C., Groves, S., & Hanson, R. 2002. Injected and remobilised Eocene sandstones from the Alba Field, UKCS: core and wireline characteristics. *Petroleum Geoscience,* **8**, 99–107.

Duranti, D. & Hurst, A. 2004. Fluidization and injection in the deep-water sandstones of the Eocene Alba Formation (UK North Sea). *Sedimentology*, **v. 51**, p. 503–529, doi: 10.1111/j.1365-3091.2004.00634.x

Ernst, W.G. 1983. Phanerozoic continental accretion and the metamorphic evolution of Northern and Central California. *Tectonophysics*, v. 100, p. 287–320.

Fisher, N. I., Lewis, T. & Embleton, B. J. J. 1987. Statistical Analysis of Spherical Data. Cambridge University Press, Cambridge. doi: 10.1017/CBO9780511623059

Flemings, P.B., Stump, B.B., Finkbeiner, T. & Zoback, M. 2002. Flow Focusing In Overpressured Sandstones: Theory, Observations, and Applications. *American Journal Of Science*, **Vol. 302**, pp. 827–855.

Graham, S.A. 1987. Tectonic controls on petroleum occurrence incentral California. *In*: Ingersoll, R.V., Ernst, W.G. (Eds.), *Cenozoic Basin Development of Coastal California*. Rubey, **vol. 6**. Prentice-Hall, Englewood Cliffs, pp. 47-63.

Grippa, A., Hurst, A., Palladino, G., Iacopini, D., Lecomte, I. & Huuse, M. 2019. Seismic imaging of complex geometry: Forward modeling of sandstone intrusions. *Earth and Planetary Science Letters*, 513, 51–63, https://doi.org/10.1016/j.epsl.2019.02.011.

Harms, T.A., Jayko, A.S. & Blake, M.C. 1992. Kinematic evidence for extensional unroofing of the franciscan complex along the coast range fault, northern diablo range, California. *Tectonics*, v. **11**, p. 228–241. https://doi.org/10.1029/91TC01880.

He, M., Graham, S., Scheirer, A.H. & Peters, K.E. 2014. A basin modeling and organic geochemistry study in the Vallecitos syncline, San Joaquin Basin, California. *Marine and Petroleum Geology*, **v. 49**, p. 15–34, doi: 10.1016/j.marpetgeo.2013.09.001

Hubbard, S.M., Romans, B.W. & Graham, S.A. 2007. An outcrop example of large-scale conglomeratic intrusions sourced from deep-water channel deposits, Cerro Toro Formation, Magallanes basin, southern Chile. *In*: Hurst, A., Cartwright, J. (Eds.), *Sand Injectites: Implications for Hydrocarbon Exploration and Production.* American Association of Petroleum Geologists Memoir, Tulsa, pp. 199–207.

Hurst, A., Cartwright, J.A., Huuse, M., Jonk, R., Schwab, A.M., Duranti, D. & Cronin, B.T. 2003a. Significance of large-scale sand injectites as long-term fluid conduits: evidence from seismic data. *Geofluids* 3, 263-274.

Hurst, A., Cartwright, J. & Duranti, D. 2003b. *Fluidization structures produced by upward injection of sand through a sealing lithology*. Geological Society, London, Special Publications, **v. 216**, p. 123–138, doi: 10.1144/GSL.SP.2003.216.01.09.

Hurst, A., Cartwright, J.A., Duranti, D., Huuse, M. & Nelson, M. 2005. Sand injectites: an emerging global play in deep-water clastic environments. *In*: Doré, A., Vining, B. (Eds.), *Petroleum Geology: North-west Europe and Global Perspectives. Proceedings of the 6th Petroleum Geology conference*. Geological Society, London, pp. 133–144.

Hurst, A., Cartwright, J.A., Huuse, M. & Duranti, D. 2006. Extrusive sandstones (extrudites): a new class of stratigraphic trap? *In*: Allen, M.R., Goffey, G.P., Morgan, R.K., Walker, I.M. (Eds.), *The Deliberate Search for the Stratigraphic Trap*. Geological Society, London, Special Publications, **vol. 254**., pp. 289–300.

Hurst, A., Huuse, M., Cartwright, J. & Duranti, D. 2007. Sand Injectites in Deep-water Clastic Reservoirs: Are They There and Do They Matter ? *Atlas of deep-water outcrops: AAPG Studies in Geology*, **56**, p. 1–24.

Hurst, A. & Cartwright, J. 2007. Relevance of Sand Injectites to Hydrocarbon Exploration and Production. *In:* Hurst, A. & Cartwright, J. (eds) *Sand injectites: Implications for hydrocarbon exploration and production*. AAPG Memoir, **87**, p. 1–19, doi: 10.1306/1209846M871546.

Hurst, A., Scott, A. & Vigorito, M. 2011. Physical characteristics of sand injectites. *Earth-Science Reviews*, **v. 106**, p. 215–246, doi: 10.1016/j.earscirev.2011.02.004

Hurst, A., Huuse, M., Duranti, D., Vigorito, M., Jameson, E. & Schwab, A. 2016. Application of outcrop analogues in successful exploration of a sand injection complex, Volund Field, Norwegian North Sea. *Geological Society, London. Special Publications, 436. http://dx.doi.org/10.1144/SP436.3*

Hurst, A. & Vigorito, M. 2017. Saucer-shaped sandstone intrusions: An underplayed reservoir target. *AAPG Bulletin*, **v. 101**, p. 625–633, doi: 10.1306/011817DIG17070

Hurst, A., Morton, A., Scott, A. & Vigorito, M. 2017. Heavy-mineral assemblages in sandstone intrusions : panoche giant injection complex , California , U.S.A.. *Journal of Sedimentary Research*, 2017, v. 87, 388–405. DOI: http://dx.doi.org/10.2110/jsr.2017.22

Huuse, M., Duranti, D., Steinsland, N., Guaranga, C.G., Prat, P., Holm, K., Cartwright, J.A. & Hurst, A. 2004. Seismic characteristics of large-scale sandstones intrusions in the Paleogene of the South Viking Graben, UK and Norwegian North Sea. *In*: Davies, R.J. Huuse, M., Cartwright, J., Hurst, A. & Steinsland, N. 2007. *Seismic Characterization of Large-scale Sandstone Intrusions: Sand injectites: Implications for hydrocarbon exploration and production*. AAPG Memoir 87, p. 21–35, doi: 10.1306/1209847M873253

Huuse, M. & Mickelson, M. 2004. Eocene sandstone intrusions in the Tampen Spur area (Norwegian North Sea Quad 34) imaged by 3D seismic data. *Marine and Petroleum Geology*, **21**, 141–155, https://doi.org/10.1016/j.marpetgeo.2003.11.018

Huuse, M., Cartwright, J.A., Gras, R. & Hurst, A. 2005. Kilometre-scale sandstone intrusions. *In*: Doré, A.G., Vining, B.A. (Eds.), *Petroleum Geology: North-West Europe and Global Perspectives–Proceedings of the 6th Petroleum Geology Conference*. Geological Society of London, pp. 1577–1594.

Huuse, M., Cartwright, J., Hurst, A. & Steinsland, N. 2007. Seismic characterization of large-scale sandstone intrusions. *In*: Hurst, A. & Cartwright, J. (Eds.), *Sand Injectites: Implications for Hydrocarbon Exploration and Production*, **vol. 87**. AAPG Memoir, pp. 21–35.

Huuse, M., Jackson, C.A.L., Van Rensbergen, P., Davies, R.J., Flemings, P.B. & Dixon, R.J. 2010. Subsurface sediment remobilization and fluid flow in sedimentary basins: An overview. *Basin Research***, v. 22**, p. 342–360, doi: 10.1111/j.1365-2117.2010.00488.x

Ingersoll, R. V., 1982. Initiation and evolution of the Great Valley forearc basin of northern and central California. *In*: Leggett, J. K. (ed), *Trench-forearc geology: sedimentation and tectonics on modern and ancient active plate margins*. Geological Society of London, Special Publications, **10**, pp. 459–467.

Ingersoll, R. V. 2008. Subduction-Related Sedimentary Basins of the USA Cordillera. In: Miall, A.D. (Ed.), *The sedimentary Basins of the United States and Canada*. In: Hsü, K.J. (Ed.), *Sedimentary Basins of the World*. Elsevier, **v. 5**, p. 395-428. doi: 10.1016/S1874-5997(08)00011-7

Jackson., C.A.-L. 2007. The geometry, distribution and development of clastic injections in slope systems: seismic examples from the Upper Cretaceous Kyrre Formation, Måløy Slope, Norwegian Margin. In: Hurst, A. & Cartwright, J. (eds) *Sand injectites: Implications for hydrocarbon exploration and production*. AAPG Memoir, 87, p. 37–48.

Jackson, C.A.L., Huuse, M. & Barber, G.P. 2011. Geometry of winglike clastic intrusions adjacent to a deep-water channel complex: Implications for hydrocarbon exploration and production. *AAPG Bulletin*, 95, 559–584, https://doi.org/10.1306/09131009157

Jenkins, O.P. 1930. Sandstone dikes as conduits for oil migration through shales. *American Association of Petroleum Geologists Bulletin*, **v. 159**, p. 605–617.

Jolly, R.J.H. & Lonergan, L. 2002. Mechanisms and controls on the formation of sand intrusions. *Journal of the Geological Society*, **v. 159**, p. 605–617, doi: 10.1144/0016-764902-155

Kane, I.A. 2010. Development and flow structures of sand injectites: The Hind Sandstone Member injectite complex, Carboniferous, UK. *Marine and Petroleum Geology*, **v. 27**, p. 1200–1215. ISSN: 0264-8172 ; DOI: 10.1016/j.marpetgeo.2010.02.009

Krueger, S.W. & Jones, D.L. 1989. Extensional fault uplift of regional Franciscan blueschists due to subduction shallowing during the Laramide orogeny. *Geology*, **v. 17**, p. 1157–1159. doi: 10.1130/0091-7613

Lewan, M.D., Dolan, M.P. & Curtis, J.B. 2014. Effects of smectite on the oil-expulsion efficiency of the Kreyenhagen Shale, San Joaquin Basin, California, based on hydrous-pyrolysis experiments. *AAPG Bulletin*, **v. 98**, p. 1091–1109, doi: 10.1306/10091313059

Lillis, P. G. & Magoon, L. B. 2007. Petroleum systems of the San Joaquin Basin province, California: Geochemical characteristics of oil types. *In*: Scheirer, A.F.D. (ed.), *Petroleum systems and geological assessment of oil and gas in the San Joaquin Province, California*. U.S. Geological Survey Professional Paper, 1713, chapter **9**, 52 p.

MacLeod, M.K., Hanson, R.A., Bell, C.R. & McHugo, S. 1999. The Alba Field ocean bottom cable seismic survey: Impact on development. *The Leading Edge*, **v. 18**, p. 1306–1312, doi: 10.1190/1.1438206

Mangerud, G., Dreyer, T., Søyseth, L., Martinsen, O. & Ryseth, A. 1999. High-resolution biostratigraphy and sequence development of the Palaeocene succession, Grane Field, Norway. *Geological Society, London, Special Publications*, **152**, 167-184. https://doi.org/10.1144/GSL.SP.1999.152.01.10

McGuire, D.J., 1988. *Stratigraphy, depositional history, and hydrocarbon source-rock potential of the Upper Cretaceous–Lower Tertiary Moreno Formation, central San Joaquin basin, California* [Ph.D. thesis]: Stanford University, 309 p.

McKie, T., Rose, P.T.S., Hartley, A.J., Jones, D.W. & Armstrong, T.L. 2015. Tertiary deep-marine reservoirs of the North Sea region: an introduction. *Geological Society, London, Special Publications*, **403**, 1-16, 20, https://doi.org/10.1144/SP403.12

Milam, R.W. 1985. *Biostratigraphy and sedimentation of the Eocene and Oligocene Kreyenhagen Formation, central California*. PhD thesis, Stanford University, Stanford, 240 p.

Monnier, D., Gay, A., Imbert, P., Cavailhes, T., Soliva, R. & Lopez, M. 2015. Sand injectites network as a marker of the palaeo-stress field, the structural framework and the distance to the sand source: Example in the Vocontian Basin, SE France. *Journal of Structural Geology*, 79, 1–18, https://doi.org/10.1016/j.jsg.2015.07.001.

Morton, A., Mcfadyen, S., Hurst, A., Pyle, J. & Rose, P. 2014. Constraining the origin of reservoirs formed by sandstone intrusions: insights from heavy mineral studies of the Eocene in the Forties area, United Kingdom central North Sea. *AAPG Bulletin*, **98**, 545–561.

Namson, J.S. & Davis, T.L. 1988. Seismically active fold and thrust belt in the San Joaquin Valley, central California Seismically active fold and thrust belt in the San Joaquin Valley, central California. *Geological Society of America Bulletin*, **v. 100**, p. 257–273. doi: 10.1130/0016-7606(1988)100<0257.

Nilsen, T.H., Dibblee, T.W., J. & Simoni, T.R. 1974. Stratigraphy and sedimentology of the Cantua Sandstone Member of the Lodo Formation, Vallecitos Area, California. *SEPM Pacific Section Volume and Guidebook*, p. 38–68.

OilVoice 2013. Solimar *Energy Kreyenhagen project area joint venture status and operational update*. http://www.4-traders.com/news/Oil-Shale-activity escalating-round-Kreyenhagen-Project--14203379/

Osborne, M.J. & Swarbrick, R.E. 1997. Mechanisms for generating overpressure in edimentary basins: A reevaluation. *American Association of Petroleum Geologists,* **81**, p. 1023–1041.

Palladino, G., Grippa, A., Bureau, D., Ian, G., Alsop, Hurst, A., 2016. Emplacement of sandstone intrusions during contractional tectonics. *Journal of Structural Geology,* v. **89**, 230–249. doi: 10.1016/j.jsg.2016.06.010

Palladino, G., Alsop, G.I., Grippa, A., Zvirtes, G., Phillip, R.P. & Hurst, A. 2018. Sandstone-filled normal faults: A case study from central California. *Journal of Structural Geology*, **v. 110**, p. 86–101, doi: 10.1016/j.jsg.2018.02.013

Parize, O. & Friès, G. 2003. The Vocontian clastic dykes and sills: a geometric model. *In*: Van Rensbergen, P., Maltman, A.J., Morely, C.J. (Eds.), *Sub-surface sediment mobilization.* Geological Society of London Special Publication, **216**, pp. 51–72.

Parize, O., Beaudoin, B., Eckert, S., Fries, G., Hadj-hassen, F., Schneider, F., Su, K., Tijani, A., Trouliller, A., De Fouquet, C. & Vandromme, R. 2007. The Vocontian Aptian and Albian syndepositional clastic sills and dikes: A field-based mechanical approach to predict and model the early fracturing of marly-limy sediments. *In*: Hurst, A., Cartwright, J. (Eds.), *Sand Injectites: Implications for Hydrocarbon Exploration and Production: American Association of Petroleum Geologists Memoir*, Tulsa, pp. 163–173

Payne, M.B. 1951. Type Moreno Formation and overlying Eocene strata on the west side of the San Joaquin Valley, Fresno and Merced Counties. *California Division of Mines, Geological Special Report*, **9**.

Peters, K.E., Magoon, L.B., Valin, Z. C. & Lillis, P.G. 2007a. Source-rock geochemistry of the San Joaquin Basin Province, California. *In*: Scheirer, A.F. (Ed.), *Petroleum systems and geologic assessment of oil and gas in the San Joaquin province, California*. U.S. Geological Survey Professional Paper 1713, chapter 11, 102 p.

Peters, K.E., Magoon, L.B., Lampe, C., Hosford Scheirer, A., Lillis, P.G., & Gautier, D.L. 2007b. A four-dimensional petroleum systems model for the San Joaquin Basin province, California. *In*: Scheirer, A.F. (Ed.), *Petroleum systems and geologic assessment of oil and gas in the San Joaquin province, California*. U.S. Geological Survey Professional Paper 1713, chapter 12, 35 p.

Phillips, F.J., Tipton, A. & Watkins, R. 1974. Outcrop studies of the Eo-Oligocene Tumey Formation, Monocline Ridge, Fresno County, California: *In*, Payne, Max (fiel dtrip chairman), The Paleogene of the Panoche Creek – Catua Creek Area Central California. *Geological Guide Book for the 1974 Fall Field Trip of the Pacific Section Society of Economic Paleontologists and Mineralogists*, p. 99-131.

Platt, J.P. 1993. Exhumation of high-pressure rocks: a review of concepts and processes: a review of concepts and processes. *Terra Nova*, **5**. 119-133.

Pollard, D.D. 1973. Derivation and evaluation of a mechanical model for sheet intrusions. *Tectonophysics*, **v. 19**, p. 233–269, doi: 10.1016/0040-1951(73)90021-8

Polteau, S., Mazzini, A., Galland, O., Planke, S. & Malthe-Sørenssen, A. 2008. Saucer-shaped intrusions: Occurrences, emplacement and implications. *Earth and Planetary Science Letters*, **v. 266,** p. 195–204, doi: 10.1016/j.epsl.2007.11.015.

Ravier, E., Guiraud, M., Guillien, A., Vennin, E., Buoncristiani, J.F. & Portier, E. 2015. Micro- to macro-scale internal structures, diagenesis and petrophysical evolution of injectite networks in the Vocontian Basin (France): Implications for fluid flow. *Marine and Petroleum Geology*, v. 64, p. 125–151, doi: 10.1016/j.marpetgeo.2015.02.040.

Satur, N. & Hurst, A. 2007. Sand-injection structures in deep-water sandstones from the Ty formation (Paleocene), Sleipner Øst field, Norwegian North Sea. *In*: Hurst, A. & Cartwright, J. (Eds.), *Sand injectites: Implications for hydrocarbon exploration and production*. AAPG Memoir 87, p. 113– 117.

Satur, N., Hurst, A., Bang, A., Skjærpe, I., and Muehlboeck, S. A., *this volume*. *Characteristics of a wing-like sandstone intrusion, Volund Field*. Geological Society, London, Spetial Publications.

Schulein, B.J. 1993. *Sedimentation and tectonics of the upper lower to lower middle Eocene Domengine Formation Vallecitos syncline, California*. M.S. thesis: Stanford, California, Stanford University, 343 p

Schwab, A.M., Jameson, E.W., & Townsley, A. 2015. Volund Field: Development of an Eocene Sandstone Injection Complex, Offshore Norway. *In*: McKie, T., Rose, P.T.S., Hartley, A.J., Jones, D. & Armstrong, T.L., (Eds.), *Tertiary Deep-Marine Reservoirs of the North Sea Region: Geological Society of London, Special Publication,* **403**, p. 1–16.

Scott, A., Vigorito, M. & Hurst, A., 2009. The Process of Sand Injection: Internal Structures and Relationships with Host Strata (Yellowbank Creek Injectite Complex, California, U.S.A.). *Journal of Sedimentary Research*, **v. 79**, p. 568–583, doi: 10.2110/jsr.2009.062.

Scott, A., Hurst, A. & Vigorito, M. 2013. Outcrop-based reservoir characterization of a kilometer-scale sand-injectite complex. *AAPG Bulletin*, **v. 97**, p. 309–343, doi: 10.1306/05141211184.

Sharman, G.R., Schwartz, T.M., Shumaker, L.E., Trigg, C.R., Nieminski, N.M., Sickmann, Z.T., Malkowski, M.A., Hourigan, J.K., Schulein, B.J. & Graham, S.A. 2017. Submarine mass failure within the deltaic Domengine Formation (Eocene), California (USA). *Geosphere,* **v. 13**, p. 950–973, doi: 10.1130/GES01442.1

Skjærpe, I., Tøllefsen, I. and Endresen, T. 2018. Developing Viper-Kobra: Maximizing Recovery by Exploiting the Unique Characteristics of the Sand Injectite Environment. *80th EAGE Conference and Exhibition*, Copenhagen, June 2018, doi: 10.3997/2214-4609.201801426

Slagle, L.P. 1979. *Depositional systems and structures of the middle Eocene Domengine-Yokut Sandstone, Vallecitos, California*. M.S. thesis, Stanford, Calif., Stanford University, 59 p.

Smyers, N.B. & Peterson, G.L., 1971. Sandstone dikes and sills in the Moreno shale, Panoche hills, California. *Geological Society of America Bulletin*, **82**, 3201–3207.

Stephens, T.L., Walker, R.J., Healy, D., Bubeck, A. & England, R.W. 2018. Mechanical models to estimate the paleostress state from igneous intrusions. *Solid Earth*, **v. 9**, p. 847–858, doi: 10.5194/se-9-847-2018.

Sullivan, R. & Sullivan, M.D. 2012. Sequence Stratigraphy and Incised Valley Architecture of the Domengine Formation, Black Diamond Mines Regional Preserve and the Southern Sacramento Basin, California, U.S.A. *Journal of Sedimentary Research*, **v. 82**, p. 781–800, doi: 10.2110/jsr.2012.66.

Surlyk, F., Gjelberg, J. & Noe-Nygaard, N. 2007. The Upper Jurassic Hareelv Formation of East Greenland: A Giant Sedimentary Injection Complex. *In:* Hurst, A. & Cartwright, J. (eds) *Sand injectites: Implications for hydrocarbon exploration and production*. AAPG Memoir, **87**, p. 141–149.

Szarawarska, E., Huuse, M., Hurst, A., De Boer, W., Lu, L., Molyneux, S. & Rawlinson, P.B. 2010. Three-dimensional seismic characterisation of large-scale sandstone intrusions in the lower Palaeogene of the North Sea: completely injected vs. in situ remobilised sandbodies. *Basin Studies*, **22**, 517–532.

Thompson, B.J., Garrison, R.E. & Moore, C.J., 2007. A reservoir-scale Miocene Injectite near Santa Cruz, California. *In*: Hurst, A., Cartwright, J. (Eds.), *Sand Injectites: Implications for Hydrocarbon Exploration and Production*. American Association of Petroleum Geologists Memoir, Tulsa, pp. 151–162.

Todd, T.W. & Monroe, W.A. 1968. Petrology of Domengine Formation (Eocene) at Potrero Hills and Rio Vista, California. *Journal of Sedimentary Research*, **v. 38**, p. 1024–1039, doi: 10.1306/74D71AF0-2B21-11D7-8648000102C1865D.

Unruh, J., O'Connell, D. & Block, L. V. 2004. Crustal structure of the ancestral northwestern California forearc region from seismic reflection imaging: Implications for convergent margin tectonics. *Tectonophysics*, **v. 392**, p. 219–240, doi: 10.1016/j.tecto.2004.04.018.

Unruh, J.R., Dumitru, T.A. & Sawyer, T.L. 2007. Coupling of early Tertiary extension in the Great Valley forearc basin with blueschist exhumation in the underlying Franciscan accretionary wedge at Mount Diablo, California. *Bulletin of the Geological Society of America*, **v. 119**, p. 1347–1367, doi: 10.1130/B26057.1

Vétel, W. & Cartwright, J. 2010. Emplacement mechanics of sandstone intrusions: Insights from the Panoche Giant Injection Complex, California. *Basin Research*, **v. 22**, p. 783–807, doi: 10.1111/j.1365-2117.2009.00439.x.

Vigorito, M., Hurst, A., Cartwright, J.A. & Scott, A. 2008. Regional-scale subsurface sand remobilization: geometry and architecture. *Journal of the Geological Society*, **v. 165**, p. 609–612, doi: 10.1144/0016-76492007-096.

Vigorito, M. & Hurst, A. 2010. Regional sand injectite architecture as a record of pore-pressure evolution and sand redistribution in the shallow crust: insights from the Panoche Giant Injection Complex, California. *Journal of the Geological Society*, **v. 167**, p. 889–904, doi: 10.1144/0016-76492010-004.

Zimmerman, J., 1944. Tumey Sandstone (Tertiary), Fresno County, California. *Bulletin of the American Association of Petroleum Geologists*, **v. 28**, n°7, p. 953–976.

Yardley, G.S. & Swarbrick, R.E. 2000. Lateral transfer: a source of additional overpressure? *Marine and Petroleum Geology*, **17**, 523-537.

Tables

Table 1 – Main criteria for differentiation of depositional (parent) units and sandstone intrusions (low-angle to bedding), in outcrops of the TGIC.

	Depositional sandstone	Sandstone intrusions
Geometry	Common tabular and lens shape geometry (channelized). Concordant, planar tops and common continuous and irregular erosional base.	Low-angle (predominantly) bedding discordance on all margins. Sharp, irregular erosional lower and upper margins (scallops). Steps, tapering, and interconnection with other intrusive sandstone (sills and dykes).
Relationship with host strata	No deformation.	Discordant margins with host strata (fractures modified by erosion). Frequent hydraulic fracturation of host strata and minor small-scale folding (2-10 cm amplitude).
Gradation	Common grading.	Typically no gradation but occasional normal and reverse grading. Mudstone clasts along intrusion margins and irregularly distributed, sometimes concentrated, within intrusions.
Structure	Cross- and plane-parallel bedding, occasionally structureless. Disrupted, tending to eradicated, primary structures. Common formation of structureless fabric, and banding along margins.	Mainly structureless with banding commonly adjacent to upper and lower margins. Convolute folding and irregular laminae and banding adjacent to divergences with other intrusions.
Thickness	Gradual thickness decrease toward channel margins.	Abrupt thickness variation.
Sorting	Very poorly to moderately sorted, mostly poorly sorted.	Poorly to moderately sorted, mostly moderately sorted.
Grain size	Very-fine sandstone to pebbly conglomerate.	Fine- to medium-grained sand. Minor pebbles (mudstone clasts) at the margins and central portions.
Clasts	Angular to rounded clasts, mostly rounded (0.1 cm to 60 cm diameter).	Clasts with varied shapes from very angular to sub-rounded, mostly angular, (0.1 cm to 25 cm diameter).
Bioturbation	Present but uncommon.	Absent.

Table 2. *General characteristics of the Tumey Giant Injection Complex*

Sand injection complex	Parent Units	Host Strata	Predominant intrusive elements and geometry
Upper Intrusive Interval Developed at an estimated depth of 20-200m below Late Eocene unconformity	**Upper Parent Units** Isolated slope turbiditic channel-fills (up to 35 m thick). Large-scale cross-bedding and subparallel bedding with conglomeratic basal lags at the base of channels. Disruption of primary sedimentary structures by sand fluidization creating structureless sandstone and fluidization banding.	Predominance of pale grey to white bio siliceous mudstone (200m thick) rich in radiolarians and diatoms, with local plane-parallel lamination and locally disrupted by slides and slumps. Generally fractured with extensive brecciation.	Interconnected staggered and stepped sills and dykes forming saucer-shaped and wing-like intrusions (up to 12 m aperture). Intensely hydraulically fractured host biosiliceous mudstone creating extensive zones of injection breccia. Large scale jack-up of host strata; Upper zone of low aperture (0.01-0.5m) dykes in the shallowest part of the injection complex, truncated by an erosional unconformity.
Lower Intrusive Interval Developed at an estimated depth of 200-470m below Late Eocene unconformity	**Lower Parent Units** Tabular and lens-shaped base-of-slope turbiditic channels (up to 10m thick) composed of sandstone with pebbly sandstone at the base. Planar cross-bedding and plane-parallel stratification disrupted by sand fluidization, which produces structureless sandstone and fluidization banding.	Predominance of brown clay mineral rich mudstone (ca. 300m thick) with plane-parallel lamination and minor intercalation of pale bio siliceous mudstone (0.1 - 2m thick). Generally fractured with localized brecciation near contacts with sandstone intrusions.	Sill-dominated intrusive network composed of tabular and stepped sills (0.2-2m thick) interconnected with thin low- and high-angle dykes (0.1-0.5m thick). Sill-complex with multi-layered sills (up to 30m thick) extending laterally for hundreds of meters.

Figure Captions

Fig. 1 – Location and geological context of the study area. (**a**) Simplified geological map of north and central California with location of study area (Modified Dickinson & Seeley, 1979); (**b**) W-E geological cross-sections showing the tectonic evolution of the Great Valley forearc basin from Late Cretaceous to present and the relative position of the TGIC emplaced during the Eocene in the west border of the basin. (**c**) Regional geological map of the study area with the relevant stratigraphic units (modified from Bartow 1996).

Fig. 2 – (**a**) Detailed geological map of the Tumey Giant Injection Complex at Tumey Hill area showing the main depositional units and sandstone intrusions, excluding steep dykes. Note that the sandstone intrusions are schematic representations of the most expressive bodies and not true thickness. (**b**) W-E geological cross section A-B (see map for location) of the Tumey Hill area. As in **a**, the sandstone intrusions are not in real scale for visualization purposes.

Fig. 3 – Stratigraphic column of Tumey Giant Injection Complex at Tumey Hill representing the architectural organization of the complex with main injectite elements and geometries.

Fig. 4 – (**a**) Satellite image of Tumey Hill area with the location of the main log profiles presented in figure 5. (**b**) Geological interpretation of (**a**) based on detailed geological mapping. (Source: Google Earth – image with 2x vertical exaggeration).

Fig. 5 – Integrated stratigraphic log sections of the TGIC (see figure 4a for log profiles location) with geological interpretation and facies association of the main depositional and intrusive units of the complex. Note that the intrusions between logs (blue) are schematically represented for spatial and geometric visualization.

Fig. 6 – *Outcrops of the Lower Parent Units (LPU);* ***a***, ***b***, ***c***, ***d*** *and* ***e****: Outcrop zone 1 (location fig. 4a);* (**a**) *Modified depositional turbiditic sandstone with sedimentary and remobilization features (> 6 m thick), overlain by brown mudrock being intruded by dykes and sills that emanate from the turbiditic body;* (**b**) *Geologic interpretation of* **a**; (**c**) *Preserved depositional plane-parallel stratification in the central portion of the sandstone;* (**d**) *Upper erosional surface and associated parallel banding produced by sand fluidization and remobilization of the depositional sandstone;* (**e**) *Close view of the segmented dyke emanating from parent unit; (**f**), (**g**), (**h**) and (**i**): Outcrop zone 2.* (**f**) *Base of modified depositional parent unit with brecciation and intrusion of subjacent host mudrock;* (**g**) *Photo interpretation of (**f**). Note preserved plan-parallel stratification disrupted by fluidization at the base of the bed.* (**h**) *Depositional turbidite with preserved depositional structures being disrupted and modified by sandstone dyke from below;* (**i**) *Photo interpretation of (**h**). Note the jack-up structure of host mudstone due dyke emplacement, and the mudstone rafts into fluidized sandstone.*

Fig. ***7*** *– Outcrops of the lower Intrusive Interval (outcrop zone 3, cf. figure 4a for location).* (**a**) *Panorama view of the sill-dominated zone with multi-layered* sills *and interconnected dykes intruding brown mudrock.* (**b**) *Photointerpretation of (**a**);* (**c**) *Irregular sandstone intrusion with erosional curved margins;* (**d**) *Photointerpretation of (**c**);* (**e**) *Multi-layered sills with mudstone rafts;* (**f**) Stepped sill with mudstone clasts in the centre portion of the step; (**g**) Lower erosional surface of sill with the development of mudstone-clast breccia at the margin of the sill (yellow arrow).

Fig. 8 – Outcrops of the Upper Parent Units (outcrop zone 6). (**a**) Panorama view of the main turbiditic channel complex; (**b**) Picture of the turbiditic channel feeding wing-like intrusion; (**c**) Basal section of the channel with preserved large-scale cross-bedding with respective photo interpretation in (**d**). Note mudstone clast marking cross-bedding and the conglomeratic basal lag marking erosional surface inside the channel.

Fig. 9 – Stratigraphic log section of the upper parent unit (left) of figure 8 with main facies and structures, with respective outcrop pictures (right).

Fig. 10 – (**a**) Panorama view of the Upper Intrusion Interval (outcrop zones 5, 6 and 7) and respective geological interpretation (**b**). Note the intrusive network of dykes, sills and the wing-like intrusion are

fed by the underlying turbiditic channel; (**c**) 3D schematic representation of the main depositional turbiditic channel (parent unit) and associated NE-dipping wing-like intrusion.

Fig. 11 – Geological features of the wing-like intrusions in the outcrop zone 7 (named Half Dome outcrop) of the Upper Intrusive Interval; (**a**) Photomosaic with a panorama view of the wing-like intrusion and respective geological interpretation (below); (**b**) and (**c**) Pictures and respective interpretation of the stepped intrusions of the wing comprised by composite sills and dykes intruding biosiliceous mudrocks. (**d**) Feeder dykes (below) connected with thick intrusion step (above); (**e**) Staggered sills connected by irregular and segmented sandstone dyke; (**f**) Interconnection of stepped sill and dykes encompassing host mudrocks. Sandstone intrusions in (**c-f**) are highlighted in yellow.

Fig. 12 – Comparison of sandstone intrusions thickness range (left) at several (averaged) elevation levels for the TGIC dykes (green circles) and sills (blue circles). The circles represent the mean thickness of each interval analysed. Elevation intervals for the lower intrusive zone: O-100, 101-200, 201-300 (m). For the upper intrusive zone the investigated intervals were: 300-400, 400-450 and 450-500 (m). Note that in both intrusive zones the thickness of intrusions decrease upward, and both intrusive intervals present a general thinning upward of intrusions thickness.

Fig. ***13*** *– Outcrops of injection breccia zone developed into biosiliceous mudstone in the upper intrusive interval (outcrop zone 5).* (**a**) *Panorama view of the injection breccia outcrop belt;* (**b**) *Host biosiliceous mudstone intensely brecciated and injected by gray, medium-grained sandstone with varied injection breccia facies. (****c****) Triangular-shaped sandstone intrusion intruding host unit producing jigsaw structures. Note clasts of mudstone concentrated in the central portion of intrusions (yellow arrows). (****d****) Matrix-supported injection breccia (dispersive breccia) grading upward to clast-supported injection breccia facies (blocky breccia). Note the varied shapes and size of clasts in a chaotic disposition.*

Fig. ***14*** *– Injection breccia outcrops (see fig. 13a for location).* (**a**) *Complex of blocky and dispersive injection breccia facies being intruded by pure sand injections;* (**b**) *Blocky breccia with angular clasts of biosiliceous mudstone. Note the intense fracturing degree of mudstone clasts producing a range of clast shapes and sizes.* (**c**) *Crosscutting relationships between breccia facies shown in detail on* (**d**) *and* (**e**)*;* (**d**) *Upper erosional surface of pure sandstone intrusion eroding the blocky and dispersive injection breccia.* (**e**) *Sandstone sill intruding mudstone and dispersive breccia facies.*

Fig. 15 – (**a**) Late Eocene erosional unconformity at the top of the TGIC that truncates sandstone dykes and the host biosiliceous mudstone of the Kreyenhagen Shale. The erosion surface is overlain by the marine Tumey Sandstone Lentil; (**b**) Geological interpretation of (a); (**c**) Erosional contact of the Tumey Sandstone Lentil (top) truncating the biosiliceous mudstone in which sandstone intrusions are common; (**d**) Conglomerate at the base of the Tumey Sandstone Lentil with clasts of biosiliceous mudstone and of consolidated sandstone (assumed to be derived from the erosion of underlying dykes.

Fig. 16 – Back-rotated (pre-folding) structural data of the TGIC. (**a**) Lower hemisphere, equal area stereoplots of contours of poles to planes of bedding, fractures, sills and dykes. (**b**) Scattered diagram of strikes and dips of the main sandstone intrusions of the complex; (**c**) Lower hemisphere, equal area stereoplot of poles to sills and dykes; (**d**) Lower hemisphere, equal area stereoplot of poles to sills and dykes of TGIC and respective Kamb contours.

Fig. 17 – Palaeo-stress analysis of the TGIC. (a) Lower hemisphere, equal area stereoplot of contours of poles to planes of fractures (left) and dykes (right), showing the three main principal eigenvectors and eigenvalues (e1, e2 and e3), and respective relative stress vectors ($\sigma1$, $\sigma2$, and $\sigma3$). (b) Relative paleo-stress field distribution based on main dilation direction of sills and dykes. Parent units represented in blue and intrusions in black. (c) Picture of the SW-dipping wing-like intrusion (left) and structural interpretation (right) with stereoplot showing the mean wing axial plain (great circle) dipping SW and the dilation axis from wing aperture direction dipping in relative low angles (20°-30°) to NE (red dots). (d) Picture of the main NE-dipping wing (left) of the complex and structural interpretation (right) with stereoplot showing the mean wing axial plane (great circle) dipping NE and the dilation axis (red dots) from main aperture direction dipping in relative higher angles (40°- 50°) to SW.

Fig. 18 *– Comparison of architectural organization, intrusive geometries, and intrusive dimensions between the TGIC with outcrop and subsurface analogues. (**a**) Schematic 3D block diagram representing the lithostratigraphic and architectural organization of the TGIC. (**b**) Schematic geological profile representing the architectural organization of the Panoche Giant Injection Complex (PGIC). Modified from (Scott et al., 2013); (**c**) TGIC winglike intrusion system extending up to 600m crosscutting the host strata ca. 100m; (**d**) Seismic section from Volund Field, North Sea, showing steep winglike reflections emanating from depositional sand body. Respective geological interpretation (below) indicate winglike intrusions emanating from depositional sand body of Balder Formation and intruding ca. 200m of host strata . Modified from Huuse et al. (2004); (**e**) Seismic section and respective geological interpretation from the Alba Field, North Sea, showing asymmetric winglike reflectors emanating from the Eocene Nauchlan member cross-cutting ca. 150m of host strata. Modified from Duranti and Hurst (2004).*

Fig. 19 *– Integrational conceptual model for the TGIC formation. (a) Pressure-depth diagram showing the overpressure evolution the TGIC (left) and respective architectural organization (right). Relative time of events (X1, X2, X3 and X4) are represented in (c). Abbreviations: LPU, Lower Parent Unit, UPU, Upper Parent Unit; (b) Schematic 3D block-diagrams showing the tectonic setting of the San Joaquin basin during the deposition of the Kreyenhagen Shale succession. The basin was under Eocene extension with associated uplift of the Franciscan Complex, deforming underlying Cretaceous strata by low angle normal faulting in the west portion of the basin (Unruh 2007). Note that the turbidites have a general palaeocurrent to W and NW; (c) Schematic evolutionary model for TGIC formation: (i) Deposition, burial and sealing of the turbiditic channel system; (ii) lateral fluid pressure transfer by tilting of the west portion of the basin leading to up dip fluid migration (blue arrows) priming overpressure build-up of parent units, and creating NW-SE preferential stress planes; (iii) fluid overpressure overcome the lithostatic pressure (Pf > Pl), initiating hydraulic fracture of host mudstone and sand injection exploiting preferential NW-SE mechanically week planes.*

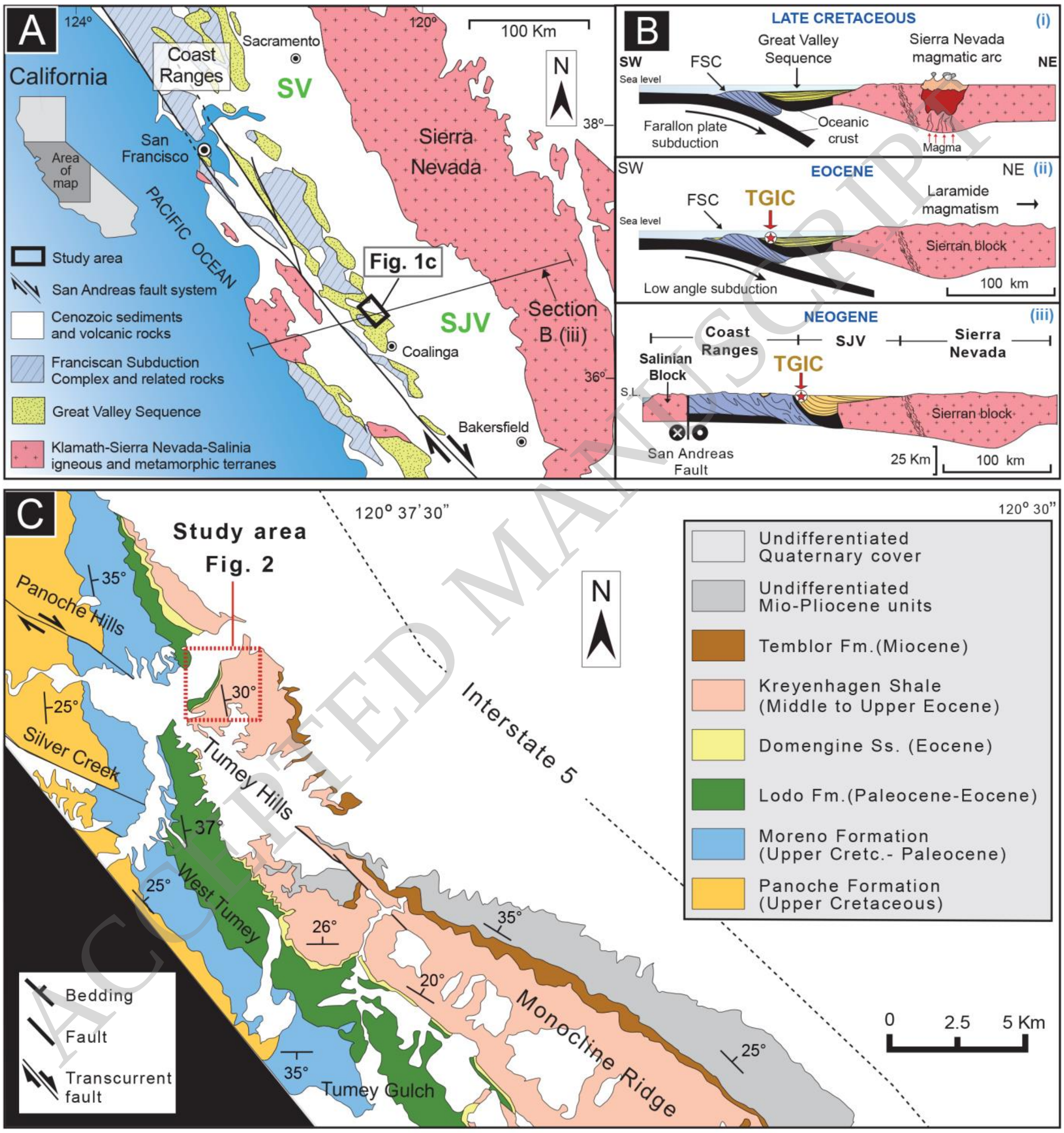
A
124°
120°
100 Km
N
38°
36°
California
Area of map
Coast Ranges
Sacramento
SV
San Francisco
Sierra Nevada
PACIFIC OCEAN
Fig. 1c
SJV
Section B.(iii)
Coalinga
Bakersfield
Study area
San Andreas fault system
Cenozoic sediments and volcanic rocks
Franciscan Subduction Complex and related rocks
Great Valley Sequence
Klamath-Sierra Nevada-Salinia igneous and metamorphic terranes
B
LATE CRETACEOUS
(i)
SW
FSC
Great Valley Sequence
Sierra Nevada magmatic arc
NE
Sea level
Farallon plate subduction
Oceanic crust
Magma
SW
EOCENE
NE
(ii)
FSC
TGIC
Laramide magmatism
Sea level
Sierran block
Low angle subduction
100 km
NEOGENE
(iii)
Coast Ranges
SJV
Sierra Nevada
Salinian Block
TGIC
S.L.
Sierran block
San Andreas Fault
25 Km
100 km
C
120° 37' 30"
120° 30"
Study area
Fig. 2
N
Interstate 5
35°
Panoche Hills
25°
30°
Silver Creek
Tumey Hills
37°
West Tumey
25°
26°
35°
20°
Monocline Ridge
25°
35°
Tumey Gulch
Undifferentiated Quaternary cover
Undifferentiated Mio-Pliocene units
Temblor Fm.(Miocene)
Kreyenhagen Shale (Middle to Upper Eocene)
Domengine Ss. (Eocene)
Lodo Fm.(Paleocene-Eocene)
Moreno Formation (Upper Cretc.- Paleocene)
Panoche Formation (Upper Cretaceous)
Bedding
Fault
Transcurrent fault
0
2.5
5 Km

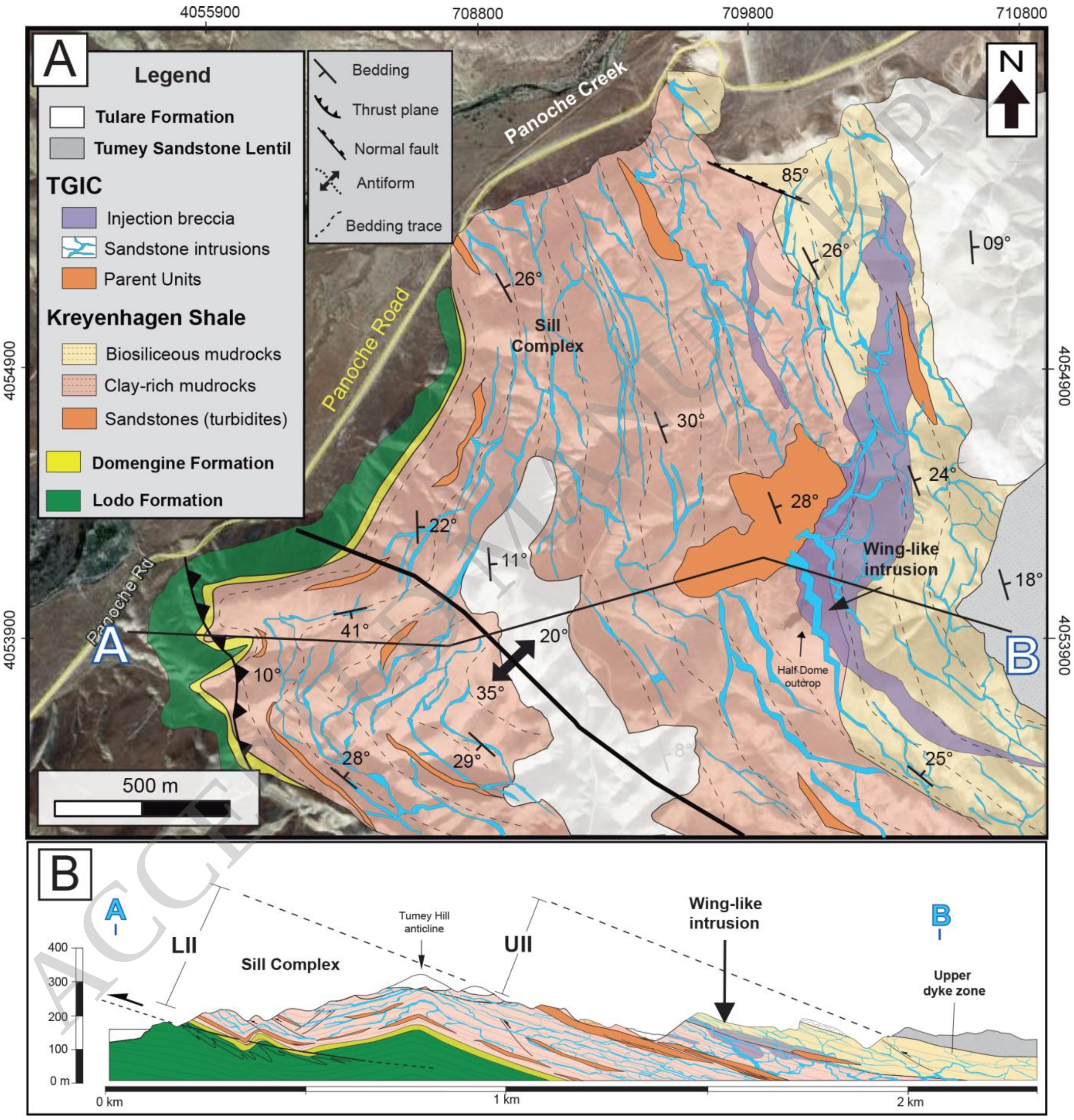
4055900
708800
709800
710800
4054900
4053900
A
Legend
Tulare Formation
Tumey Sandstone Lentil
TGIC
Injection breccia
Sandstone intrusions
Parent Units
Kreyenhagen Shale
Biosiliceous mudrocks
Clay-rich mudrocks
Sandstones (turbidites)
Domengine Formation
Lodo Formation
Bedding
Thrust plane
Normal fault
Antiform
Bedding trace
N
Panoche Creek
Panoche Road
Panoche Rd
Sill Complex
Wing-like intrusion
Half Dome outcrop
85°
26°
09°
26°
30°
24°
28°
22°
11°
18°
41°
20°
10°
35°
28°
29°
8°
25°
A
B
500 m
B
A
B
LII
UII
Sill Complex
Tumey Hill anticline
Wing-like intrusion
Upper dyke zone
400
300
200
100
0 m
0 km
1 km
2 km

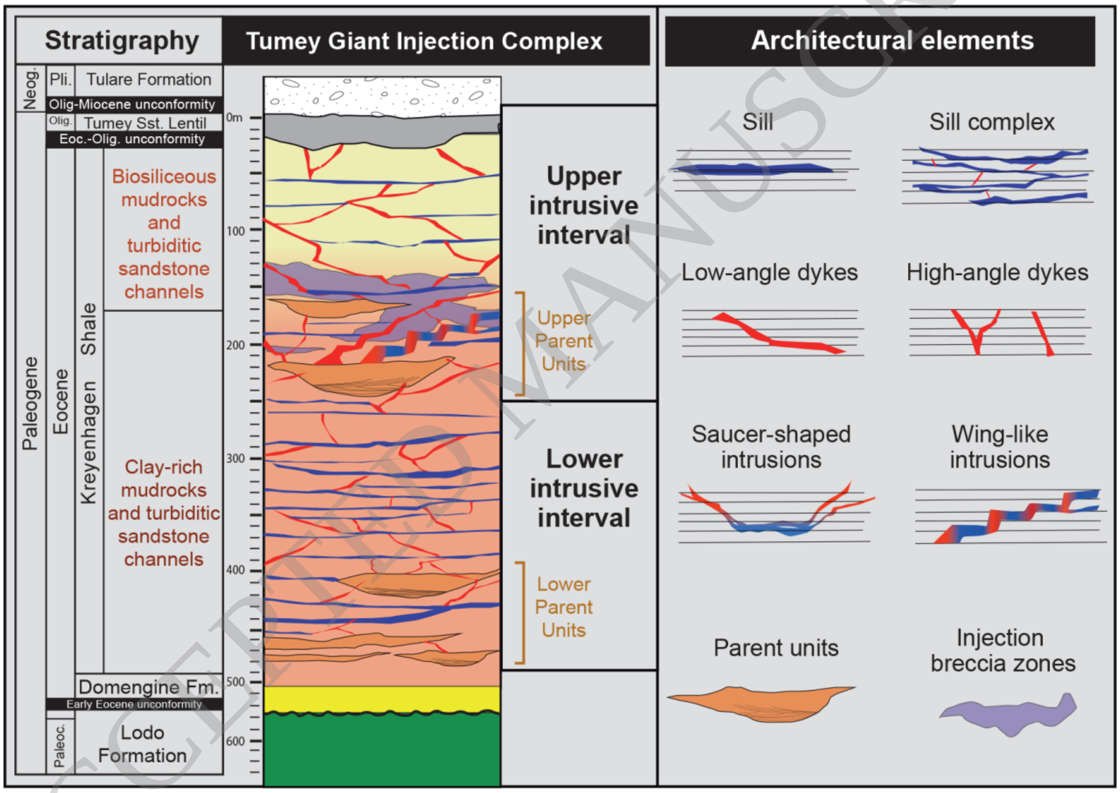
Stratigraphy
Tumey Giant Injection Complex
Architectural elements
Neog.
Pli.
Tulare Formation
Olig-Miocene unconformity
Olig.
Tumey Sst. Lentil
Eoc.-Olig. unconformity
Paleogene
Eocene
Kreyenhagen Shale
Biosiliceous mudrocks and turbiditic sandstone channels
Clay-rich mudrocks and turbiditic sandstone channels
Domengine Fm.
Early Eocene unconformity
Paleoc.
Lodo Formation
0m
100
200
300
400
500
600
Upper intrusive interval
Upper Parent Units
Lower intrusive interval
Lower Parent Units
Sill
Sill complex
Low-angle dykes
High-angle dykes
Saucer-shaped intrusions
Wing-like intrusions
Parent units
Injection breccia zones

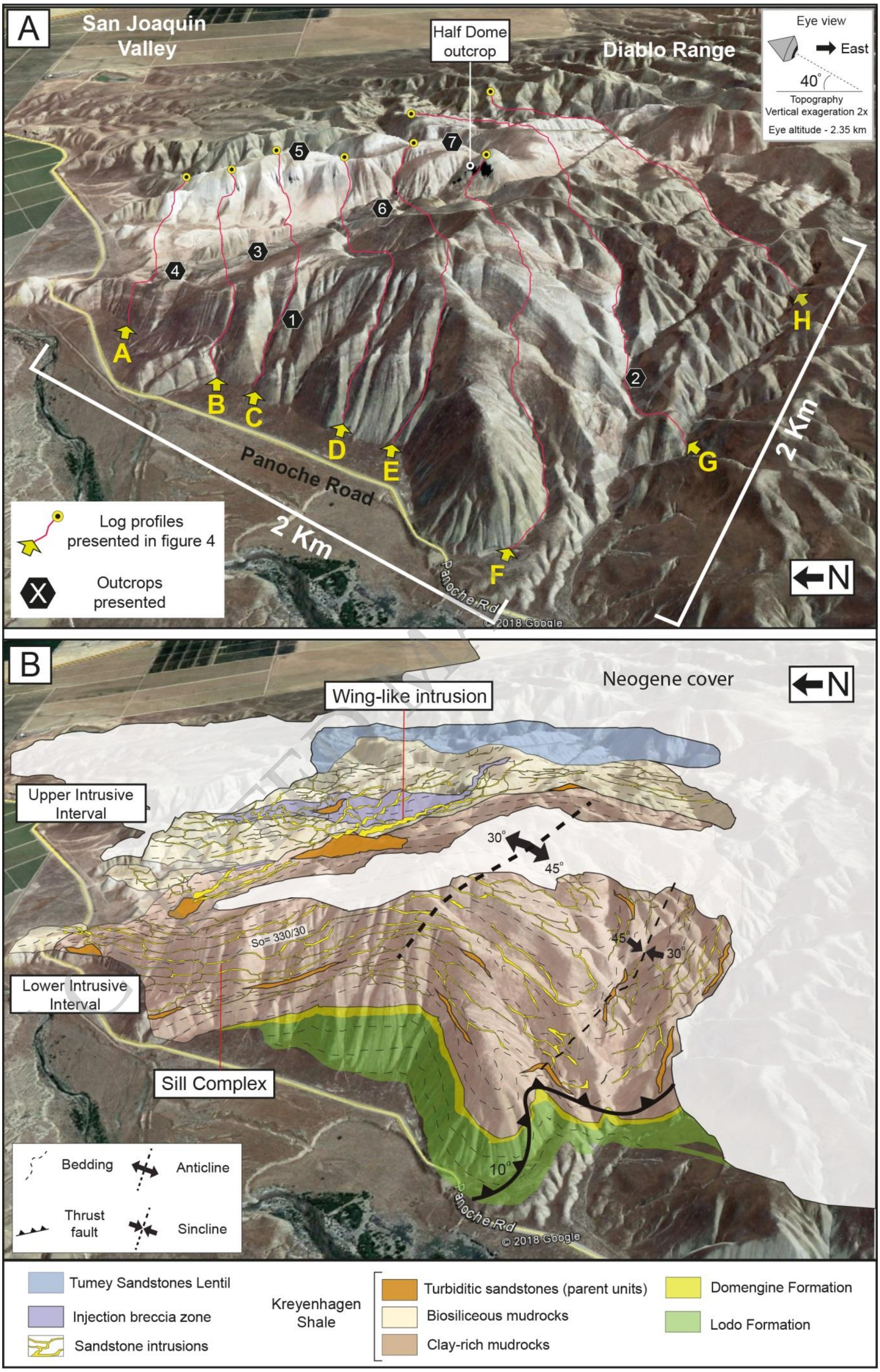
A
San Joaquin Valley
Half Dome outcrop
Diablo Range
Eye view
East
40°
Topography
Vertical exageration 2x
Eye altitude - 2.35 km
A
B
C
D
E
F
G
H
1
2
3
4
5
6
7
Panoche Road
2 Km
2 Km
Panoche Rd
N
Log profiles presented in figure 4
X
Outcrops presented
© 2018 Google
B
Wing-like intrusion
Neogene cover
N
Upper Intrusive Interval
30°
45°
So= 330/30
45°
30°
Lower Intrusive Interval
Sill Complex
10°
Bedding
Anticline
Thrust fault
Sincline
Panoche Rd
© 2018 Google
Tumey Sandstones Lentil
Injection breccia zone
Sandstone intrusions
Kreyenhagen Shale
Turbiditic sandstones (parent units)
Biosiliceous mudrocks
Clay-rich mudrocks
Domengine Formation
Lodo Formation

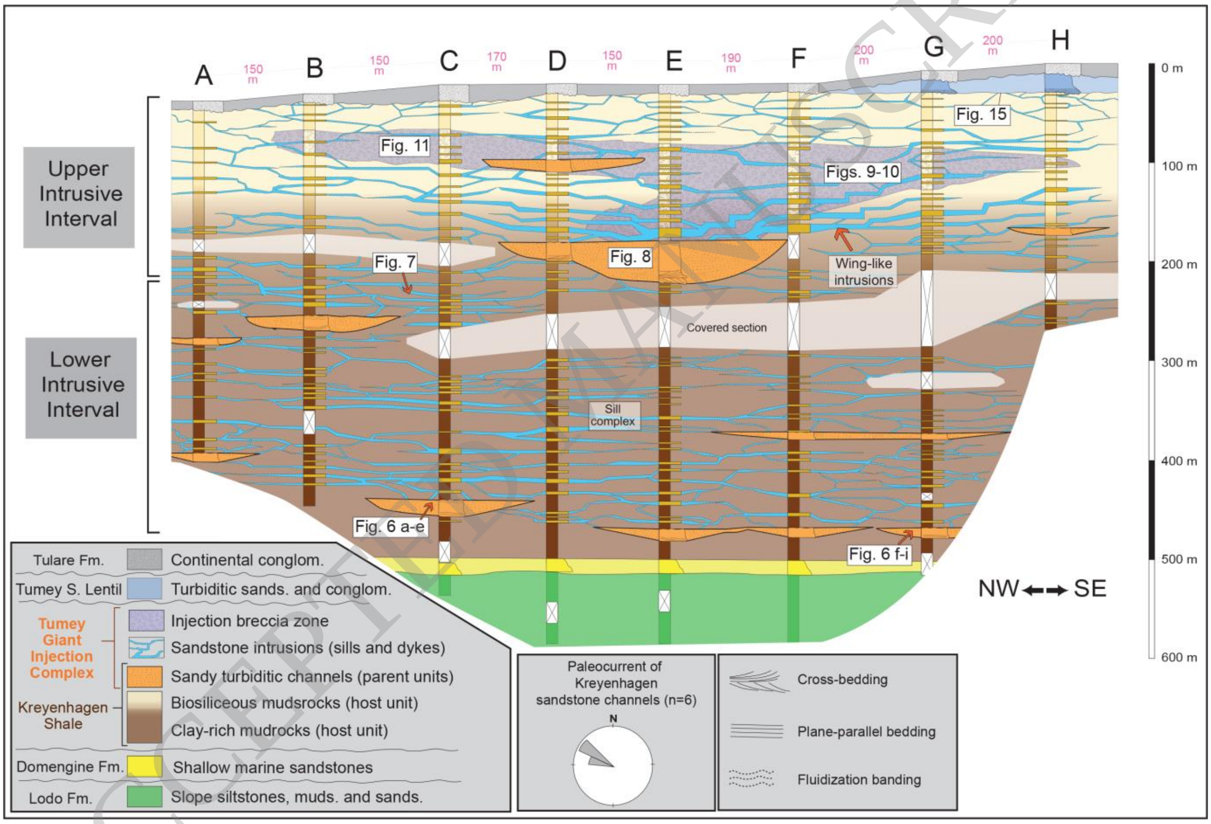
A
150 m
B
150 m
C
170 m
D
150 m
E
190 m
F
200 m
G
200 m
H
Upper Intrusive Interval
Lower Intrusive Interval
Fig. 11
Fig. 15
Figs. 9-10
Fig. 7
Fig. 8
Wing-like intrusions
Covered section
Sill complex
Fig. 6 a-e
Fig. 6 f-i
NW ← → SE
0 m
100 m
200 m
300 m
400 m
500 m
600 m
Tulare Fm.
Continental conglom.
Tumey S. Lentil
Turbiditic sands. and conglom.
Tumey Giant Injection Complex
Injection breccia zone
Sandstone intrusions (sills and dykes)
Sandy turbiditic channels (parent units)
Kreyenhagen Shale
Biosiliceous mudsrocks (host unit)
Clay-rich mudrocks (host unit)
Domengine Fm.
Shallow marine sandstones
Lodo Fm.
Slope siltstones, muds. and sands.
Paleocurrent of Kreyenhagen sandstone channels (n=6)
N
Cross-bedding
Plane-parallel bedding
Fluidization banding

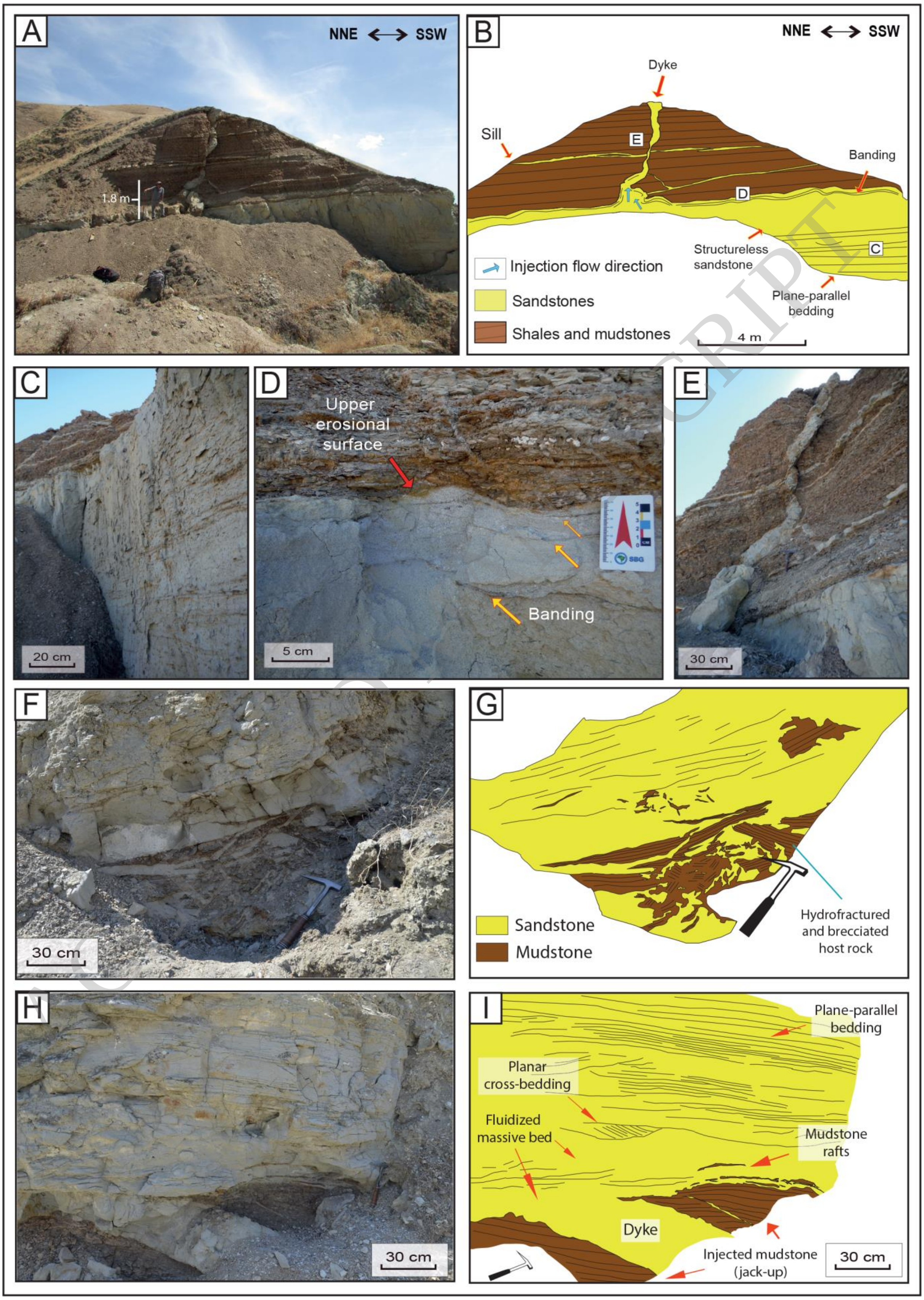
A
NNE ⟷ SSW
1.8 m
B
NNE ⟷ SSW
Dyke
Sill
E
Banding
D
C
Structureless sandstone
Plane-parallel bedding
Injection flow direction
Sandstones
Shales and mudstones
4 m
C
20 cm
D
Upper erosional surface
Banding
5 cm
E
30 cm
F
30 cm
G
Sandstone
Mudstone
Hydrofractured and brecciated host rock
H
30 cm
I
Plane-parallel bedding
Planar cross-bedding
Fluidized massive bed
Mudstone rafts
Dyke
Injected mudstone (jack-up)
30 cm

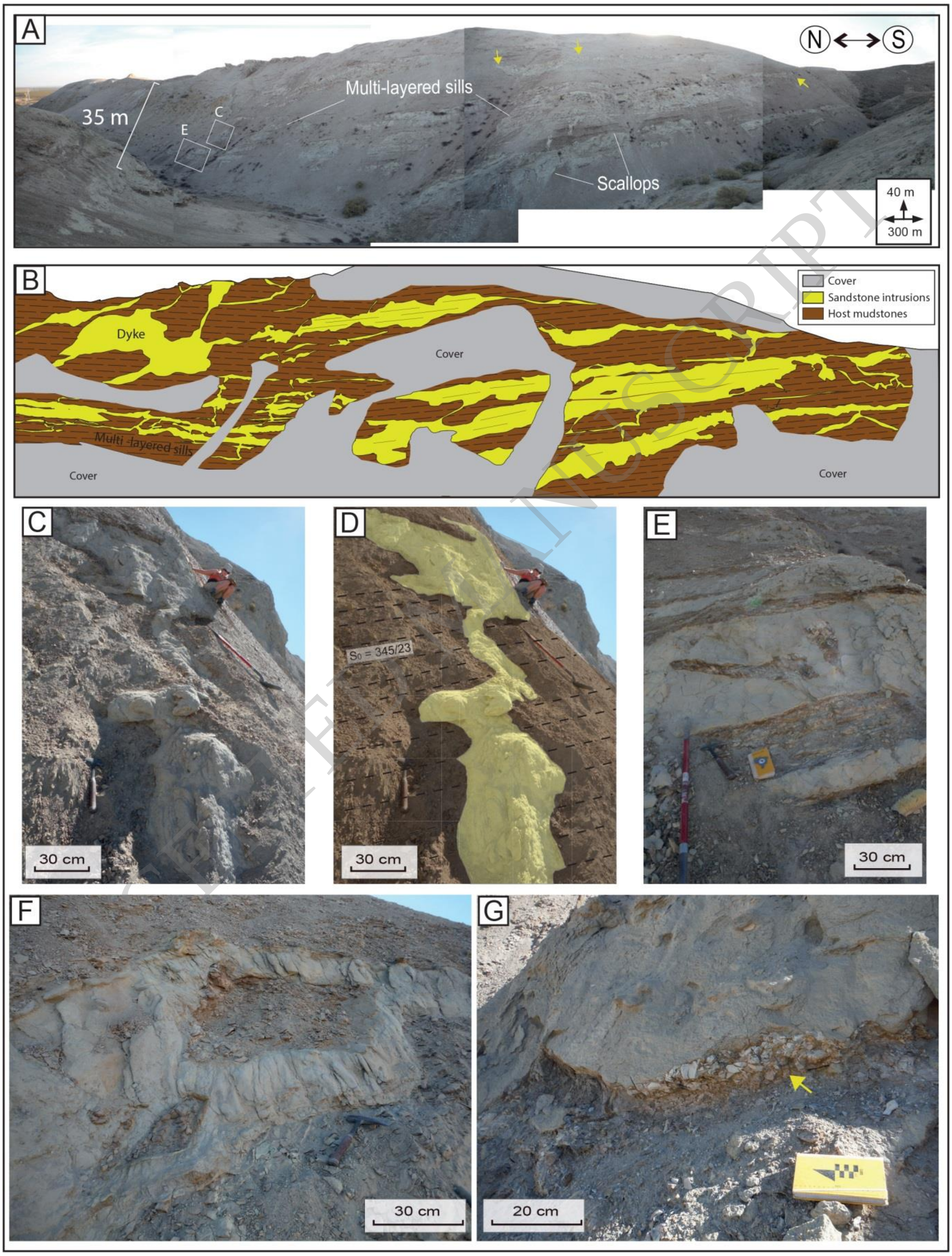
A
35 m
C
E
Multi-layered sills
Scallops
N
S
40 m
300 m
B
Cover
Sandstone intrusions
Host mudstones
Dyke
Cover
Multi -layered sills
Cover
Cover
C
30 cm
D
S0 = 345/23
30 cm
E
30 cm
F
30 cm
G
20 cm

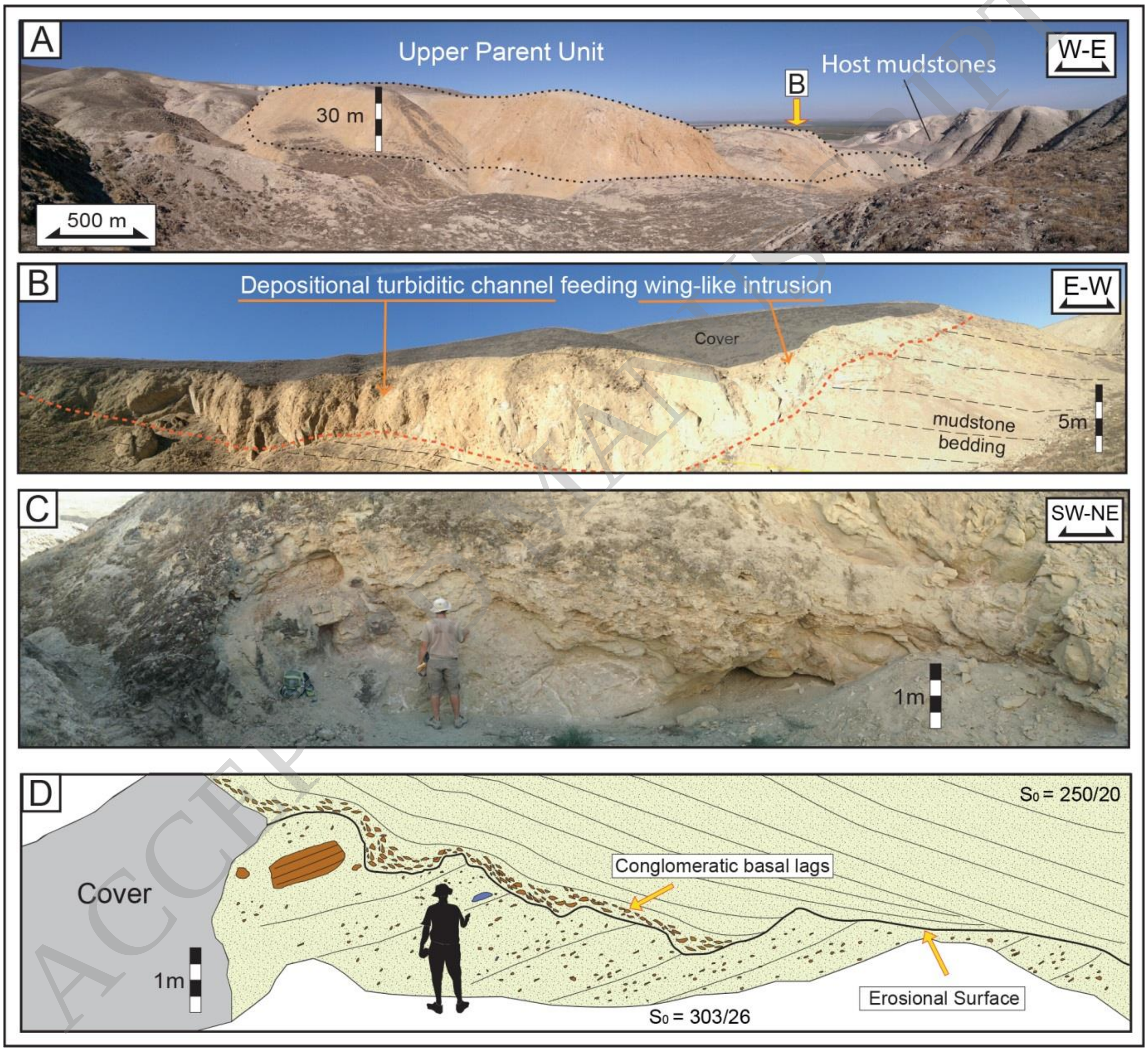
A
Upper Parent Unit
Host mudstones
W-E
B
30 m
500 m
B
Depositional turbiditic channel feeding wing-like intrusion
E-W
Cover
mudstone bedding
5m
C
SW-NE
1m
D
S0 = 250/20
Conglomeratic basal lags
Cover
1m
Erosional Surface
S0 = 303/26

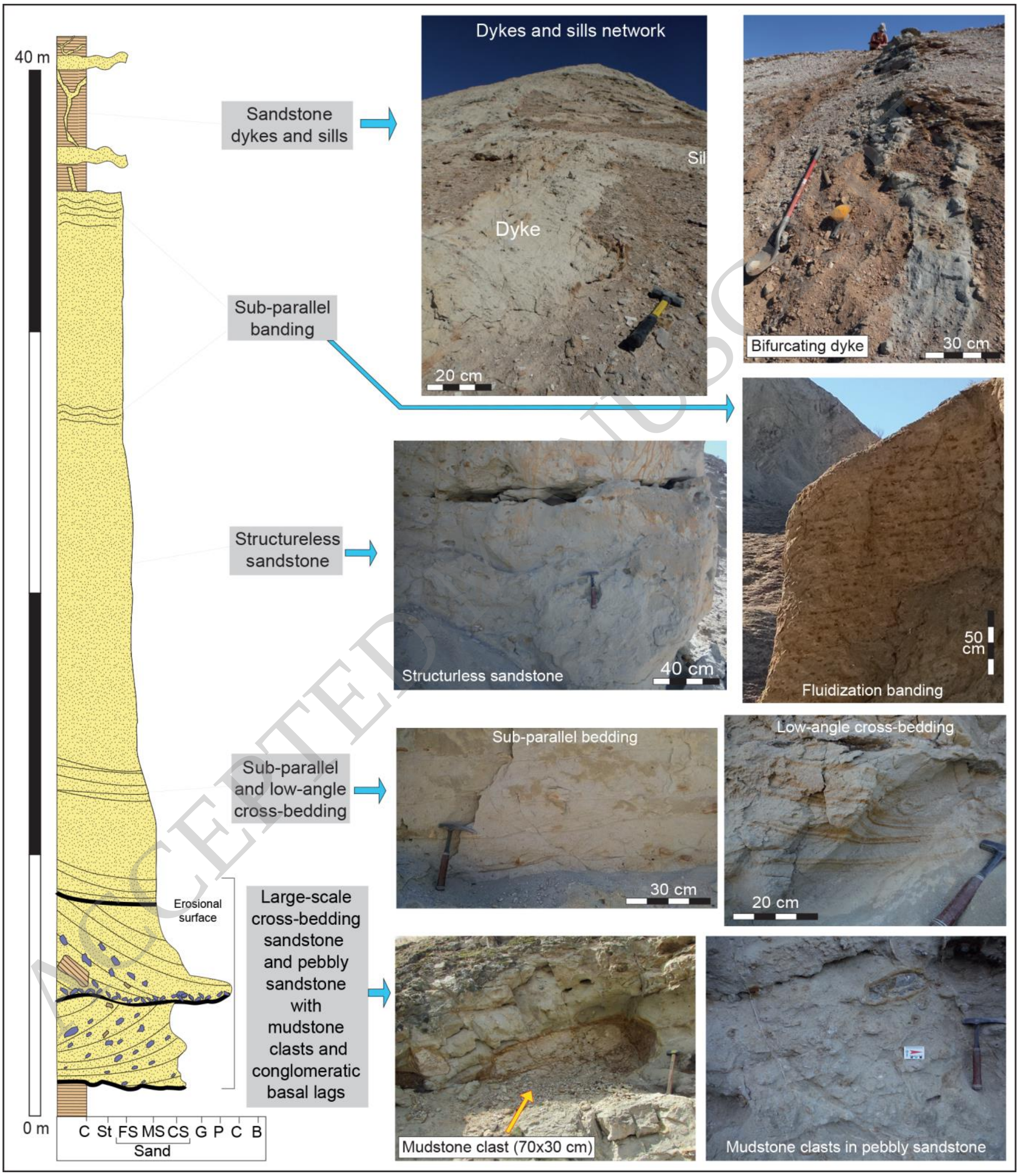
40 m
0 m
C
St
FS
MS
CS
G
P
C
B
Sand
Erosional surface
Sandstone dykes and sills
Sub-parallel banding
Structureless sandstone
Sub-parallel and low-angle cross-bedding
Large-scale cross-bedding sandstone and pebbly sandstone with mudstone clasts and conglomeratic basal lags
Dykes and sills network
Sil
Dyke
20 cm
Bifurcating dyke
30 cm
Structurless sandstone
40 cm
Fluidization banding
50 cm
Sub-parallel bedding
30 cm
Low-angle cross-bedding
20 cm
Mudstone clast (70x30 cm)
Mudstone clasts in pebbly sandstone

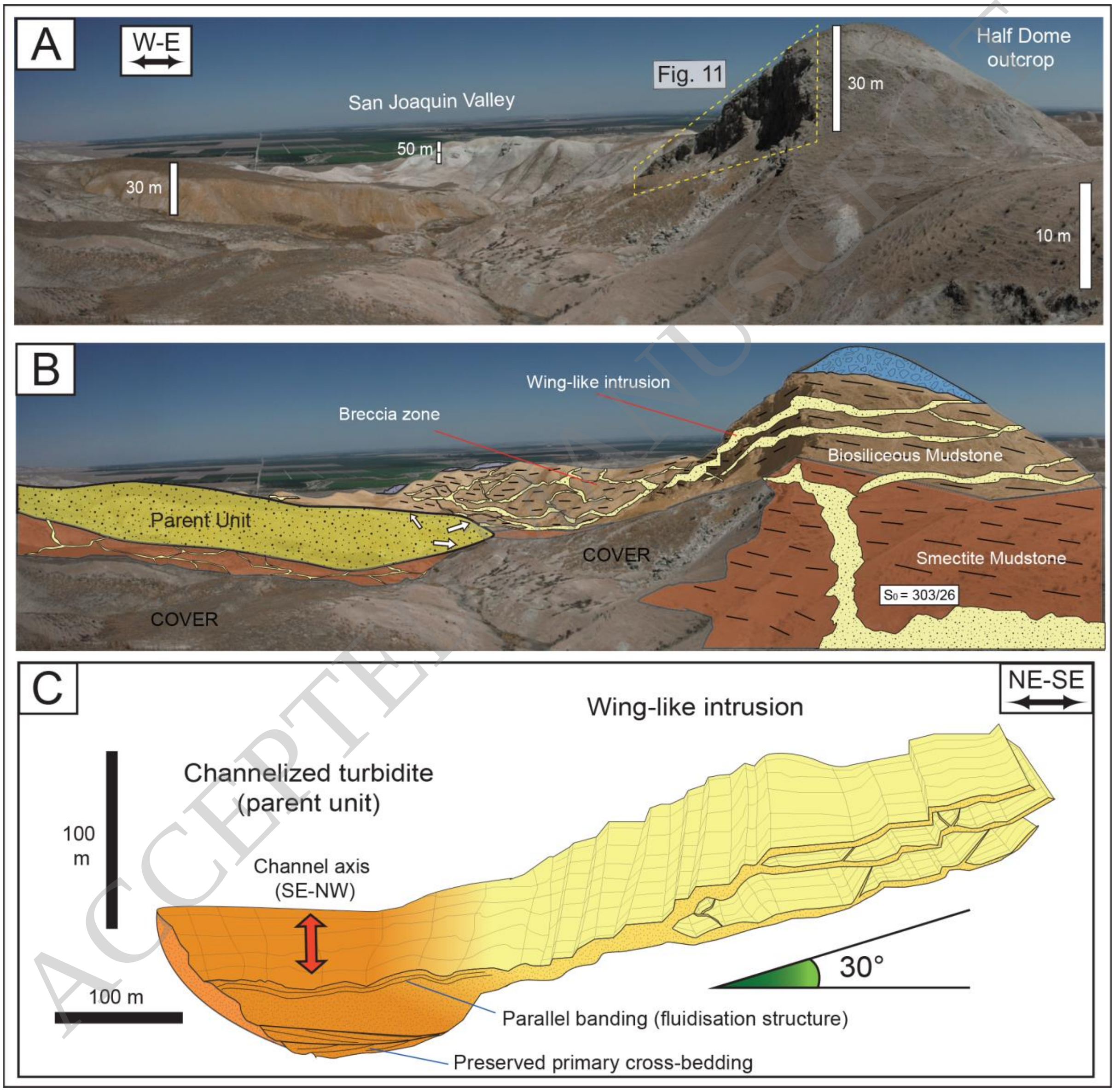
A
W-E
San Joaquin Valley
Fig. 11
Half Dome outcrop
30 m
50 m
30 m
10 m
B
Wing-like intrusion
Breccia zone
Biosiliceous Mudstone
Parent Unit
COVER
Smectite Mudstone
S_0 = 303/26
COVER
C
NE-SE
Wing-like intrusion
Channelized turbidite (parent unit)
100 m
Channel axis (SE-NW)
30°
100 m
Parallel banding (fluidisation structure)
Preserved primary cross-bedding

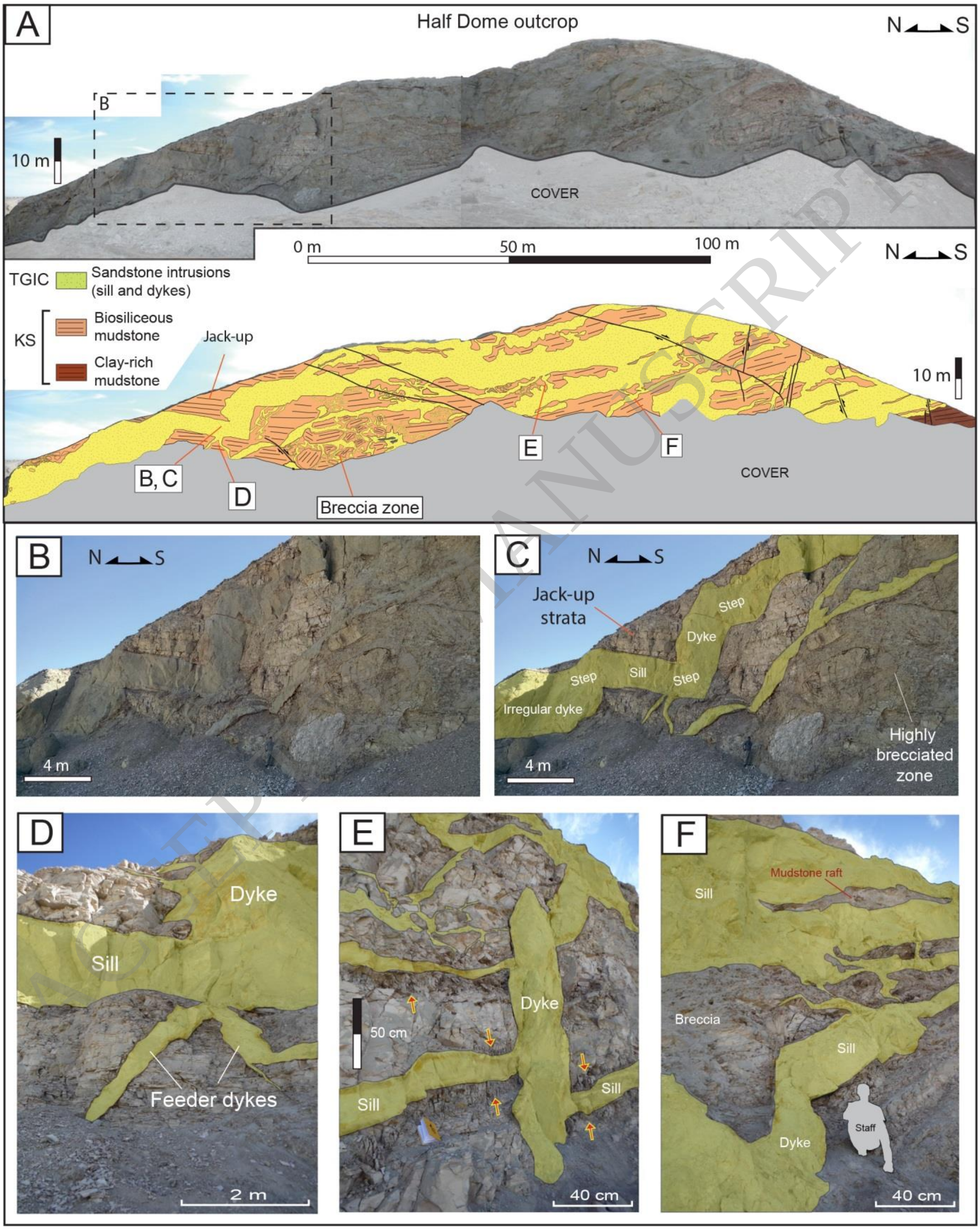
A
Half Dome outcrop
N S
B
10 m
COVER
0 m
50 m
100 m
N S
TGIC
Sandstone intrusions (sill and dykes)
KS
Biosiliceous mudstone
Clay-rich mudstone
Jack-up
10 m
E
F
B, C
D
Breccia zone
COVER
B
N S
4 m
C
N S
Jack-up strata
Step
Dyke
Step
Sill
Step
Irregular dyke
Highly brecciated zone
4 m
D
Dyke
Sill
Feeder dykes
2 m
E
Dyke
50 cm
Sill
Sill
40 cm
F
Mudstone raft
Sill
Breccia
Sill
Dyke
Staff
40 cm

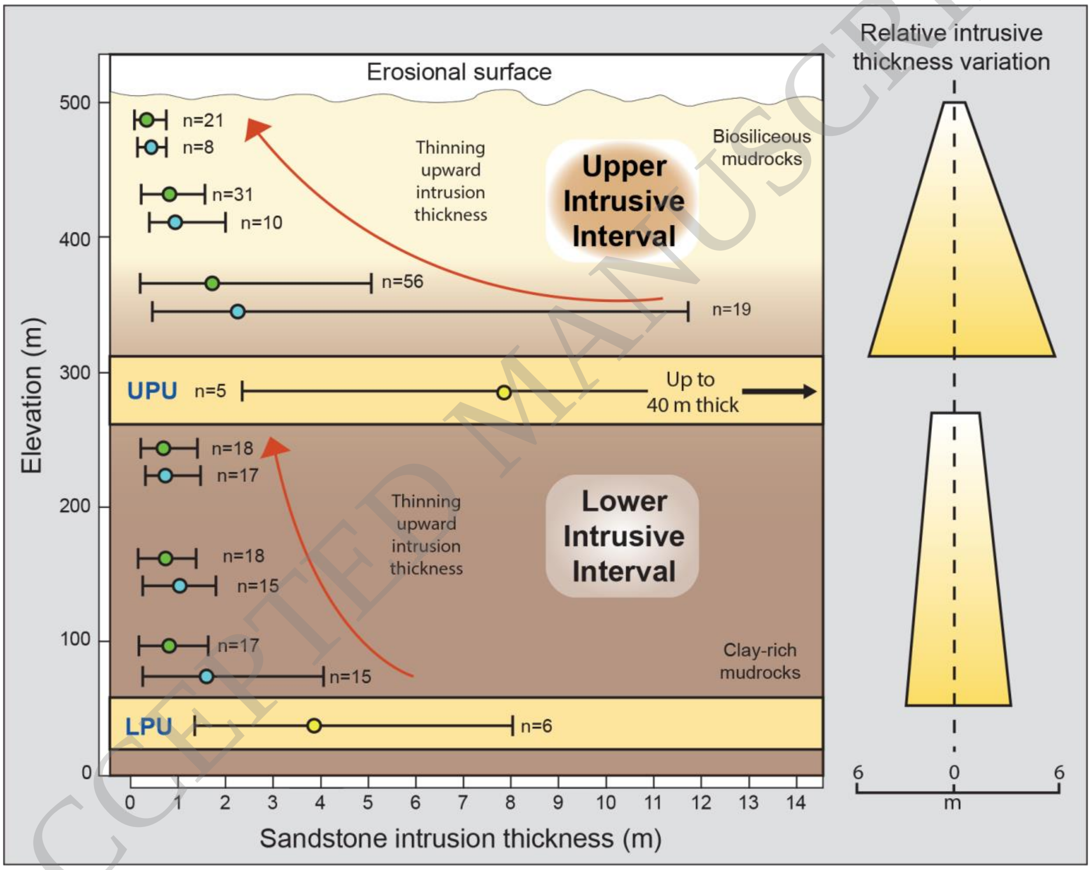
Erosional surface
Relative intrusive thickness variation
Biosiliceous mudrocks
Upper Intrusive Interval
Thinning upward intrusion thickness
n=21
n=8
n=31
n=10
n=56
n=19
UPU
n=5
Up to 40 m thick
Lower Intrusive Interval
Thinning upward intrusion thickness
n=18
n=17
n=18
n=15
n=17
n=15
Clay-rich mudrocks
LPU
n=6
Elevation (m)
0
100
200
300
400
500
Sandstone intrusion thickness (m)
0
1
2
3
4
5
6
7
8
9
10
11
12
13
14
6
0
6
m

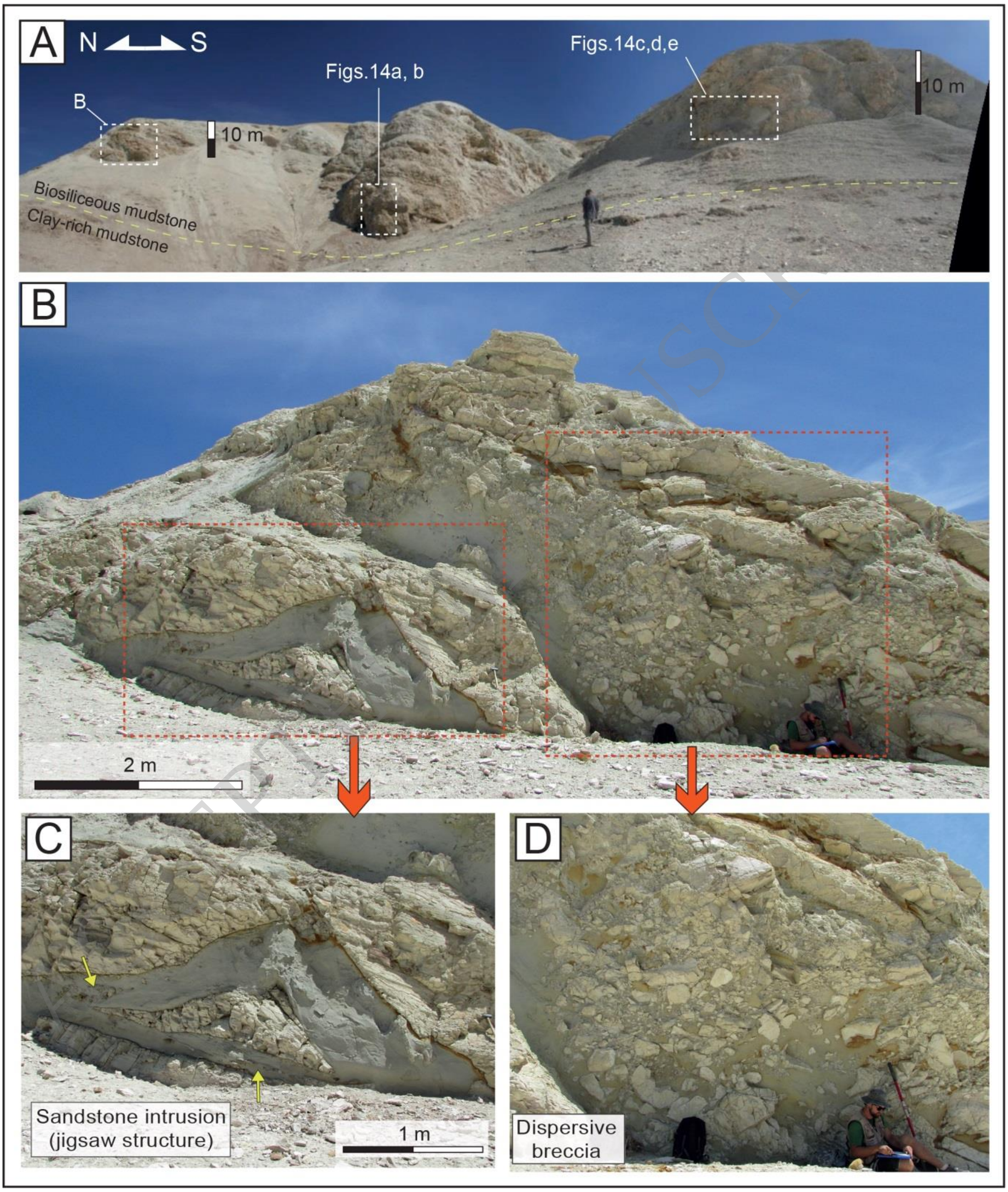
A
N
S
B
10 m
Figs.14a, b
Figs.14c,d,e
10 m
Biosiliceous mudstone
Clay-rich mudstone
B
2 m
C
Sandstone intrusion (jigsaw structure)
1 m
D
Dispersive breccia

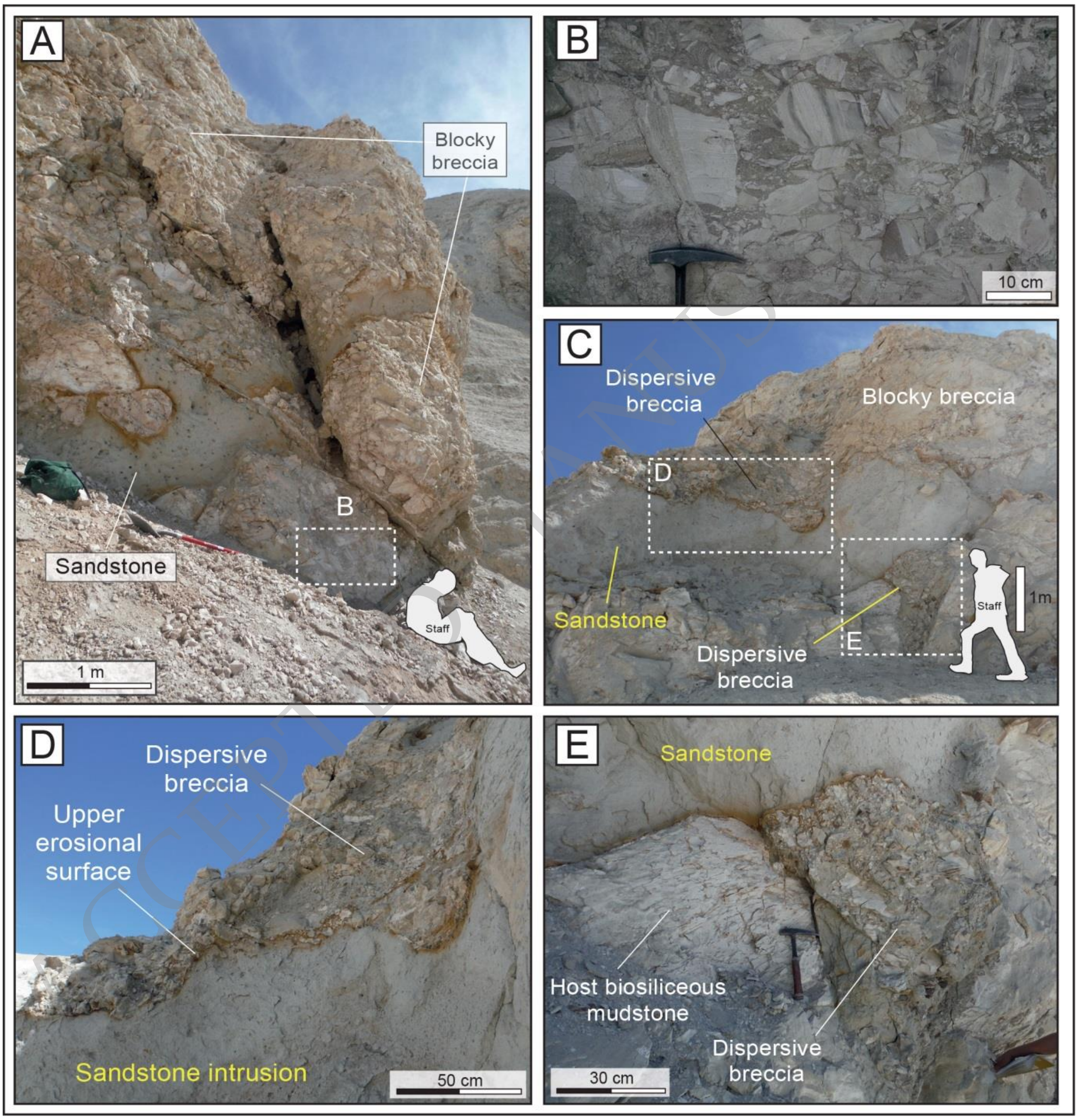
A
Blocky breccia
Sandstone
B
Staff
1 m
B
10 cm
C
Dispersive breccia
Blocky breccia
D
Sandstone
Dispersive breccia
E
Staff
1m
D
Dispersive breccia
Upper erosional surface
Sandstone intrusion
50 cm
E
Sandstone
Host biosiliceous mudstone
Dispersive breccia
30 cm

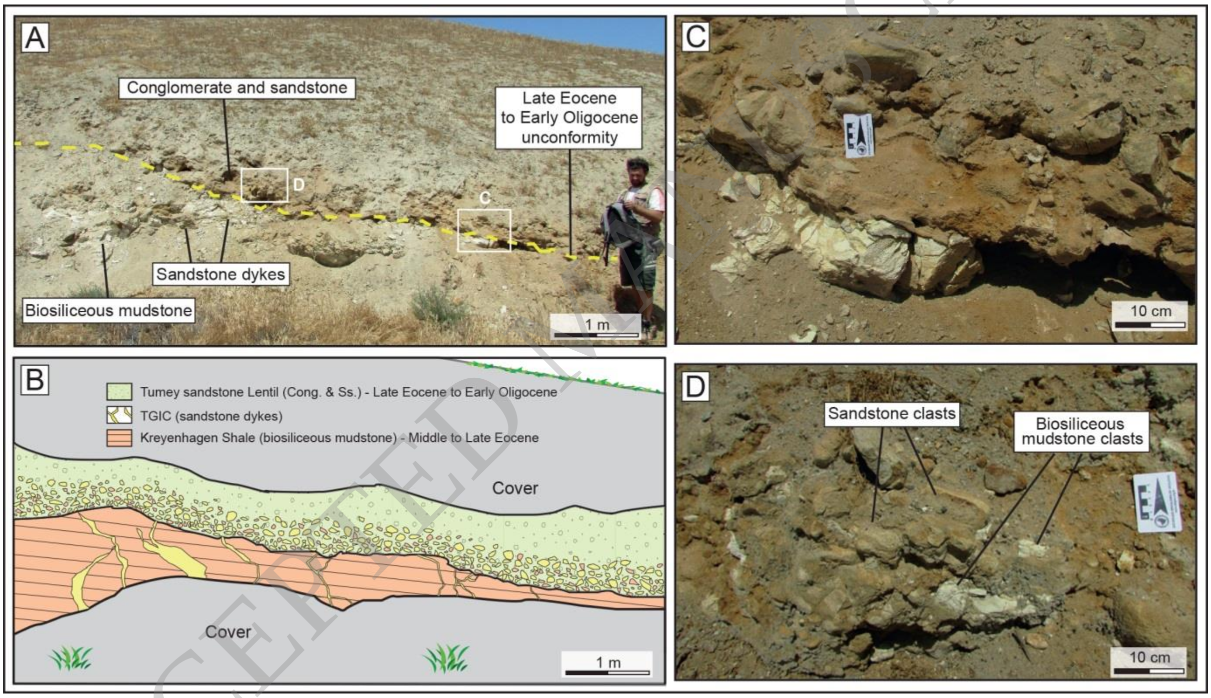
A
Conglomerate and sandstone
Late Eocene
to Early Oligocene
unconformity
D
C
Sandstone dykes
Biosiliceous mudstone
1 m
B
Tumey sandstone Lentil (Cong. & Ss.) - Late Eocene to Early Oligocene
TGIC (sandstone dykes)
Kreyenhagen Shale (biosiliceous mudstone) - Middle to Late Eocene
Cover
Cover
1 m
C
10 cm
D
Sandstone clasts
Biosiliceous
mudstone clasts
10 cm

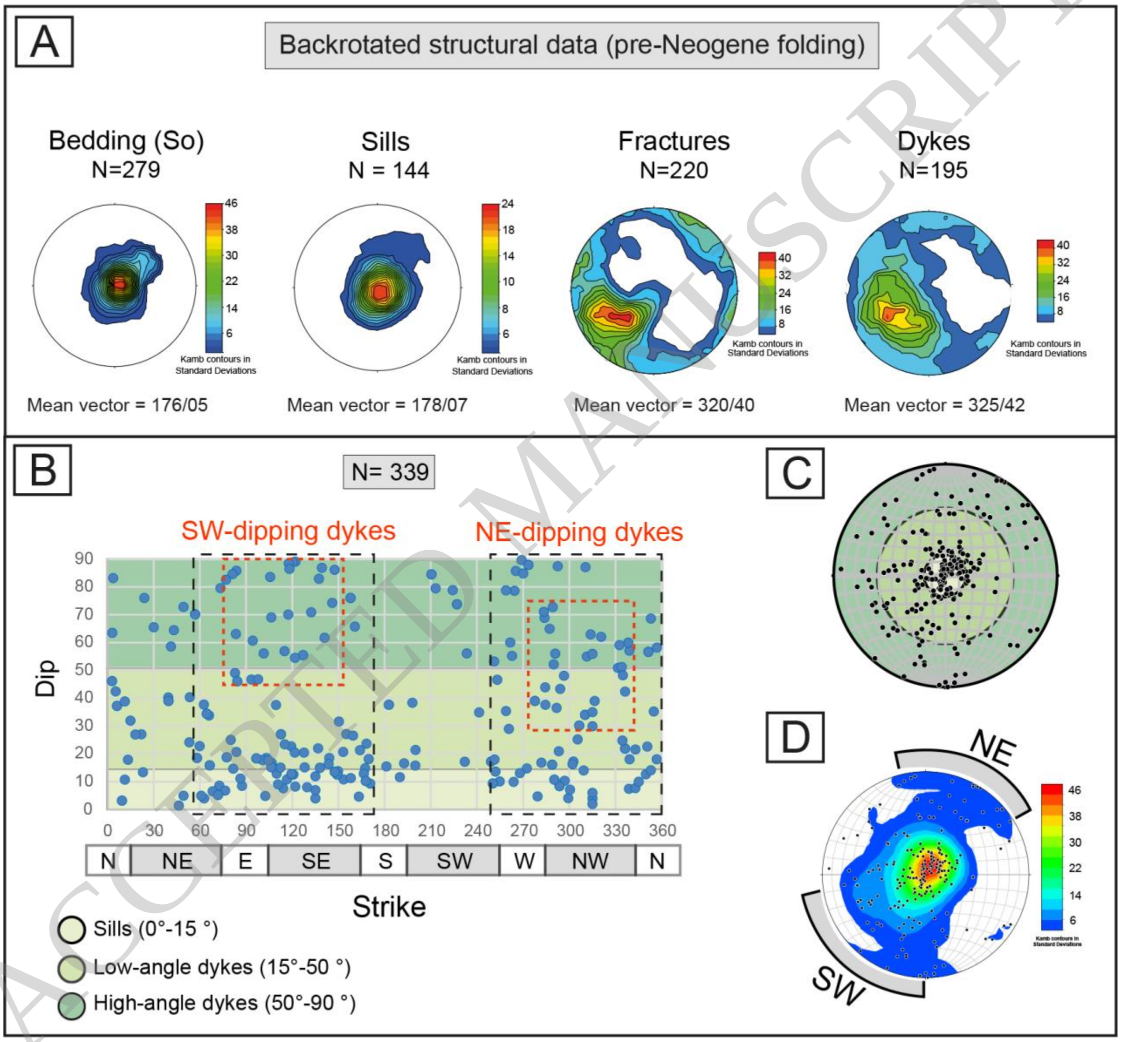
A
Backrotated structural data (pre-Neogene folding)
Bedding (So)
N=279
46
38
30
22
14
6
Kamb contours in Standard Deviations
Mean vector = 176/05
Sills
N = 144
24
18
14
10
8
6
Kamb contours in Standard Deviations
Mean vector = 178/07
Fractures
N=220
40
32
24
16
8
Kamb contours in Standard Deviations
Mean vector = 320/40
Dykes
N=195
40
32
24
16
8
Kamb contours in Standard Deviations
Mean vector = 325/42
B
N= 339
SW-dipping dykes
NE-dipping dykes
Dip
90
80
70
60
50
40
30
20
10
0
0
30
60
90
120
150
180
210
240
270
300
330
360
N
NE
E
SE
S
SW
W
NW
N
Strike
Sills (0°-15 °)
Low-angle dykes (15°-50 °)
High-angle dykes (50°-90 °)
C
D
NE
SW
46
38
30
22
14
6
Kamb contours in Standard Deviations

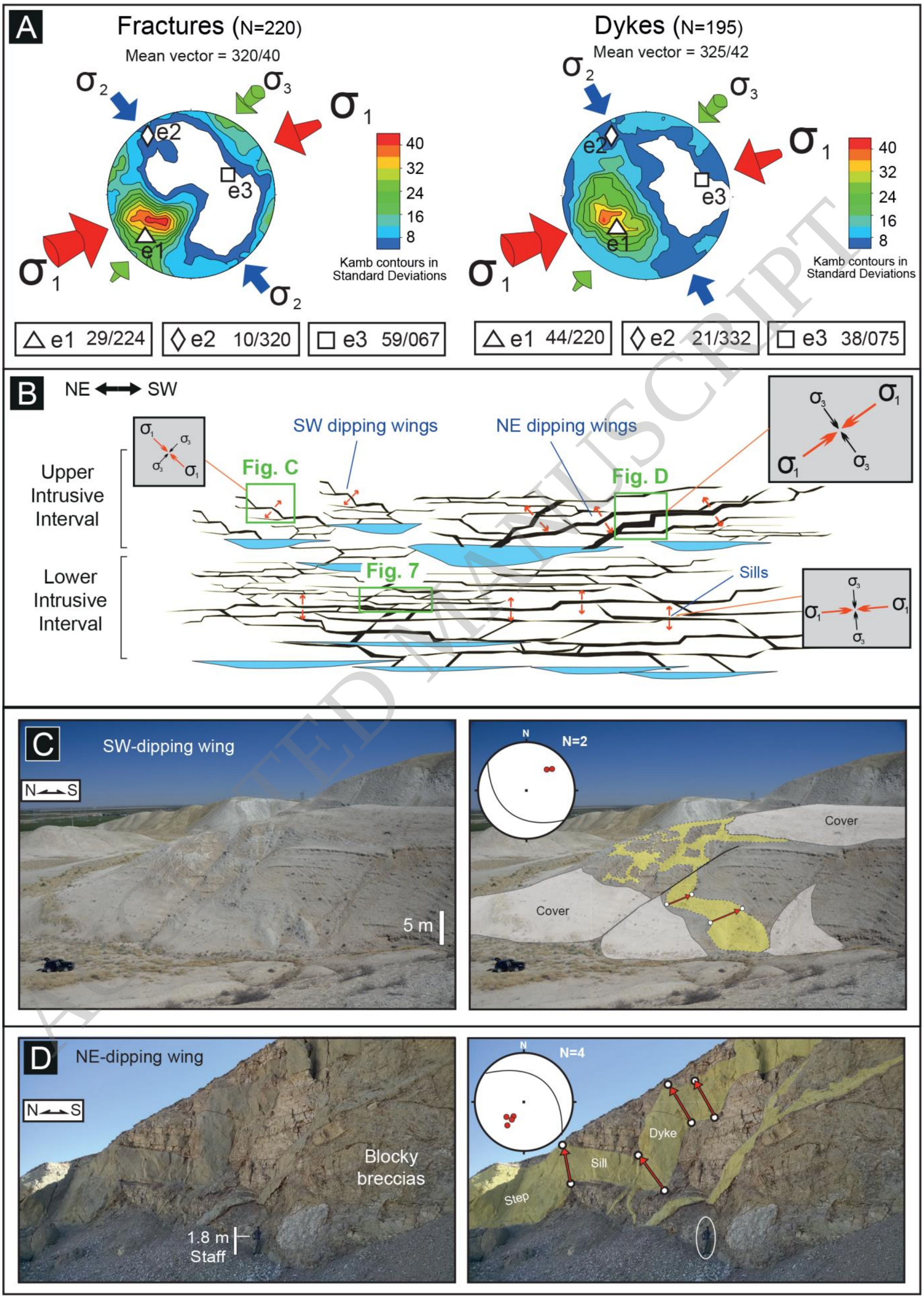
A
Fractures (N=220)
Mean vector = 320/40
σ2
σ3
σ1
e2
e3
e1
40
32
24
16
8
Kamb contours in Standard Deviations
σ1
σ2
e1 29/224
e2 10/320
e3 59/067
Dykes (N=195)
Mean vector = 325/42
σ2
σ3
σ1
e2
e3
e1
40
32
24
16
8
Kamb contours in Standard Deviations
σ1
e1 44/220
e2 21/332
e3 38/075
B
NE SW
σ1 σ3 σ3 σ1
SW dipping wings
NE dipping wings
σ3 σ1 σ1 σ3
Upper Intrusive Interval
Fig. C
Fig. D
Lower Intrusive Interval
Fig. 7
Sills
σ3 σ1 σ1 σ3
C
SW-dipping wing
N S
5 m
N
N=2
Cover
Cover
D
NE-dipping wing
N S
Blocky breccias
1.8 m Staff
N
N=4
Dyke
Sill
Step

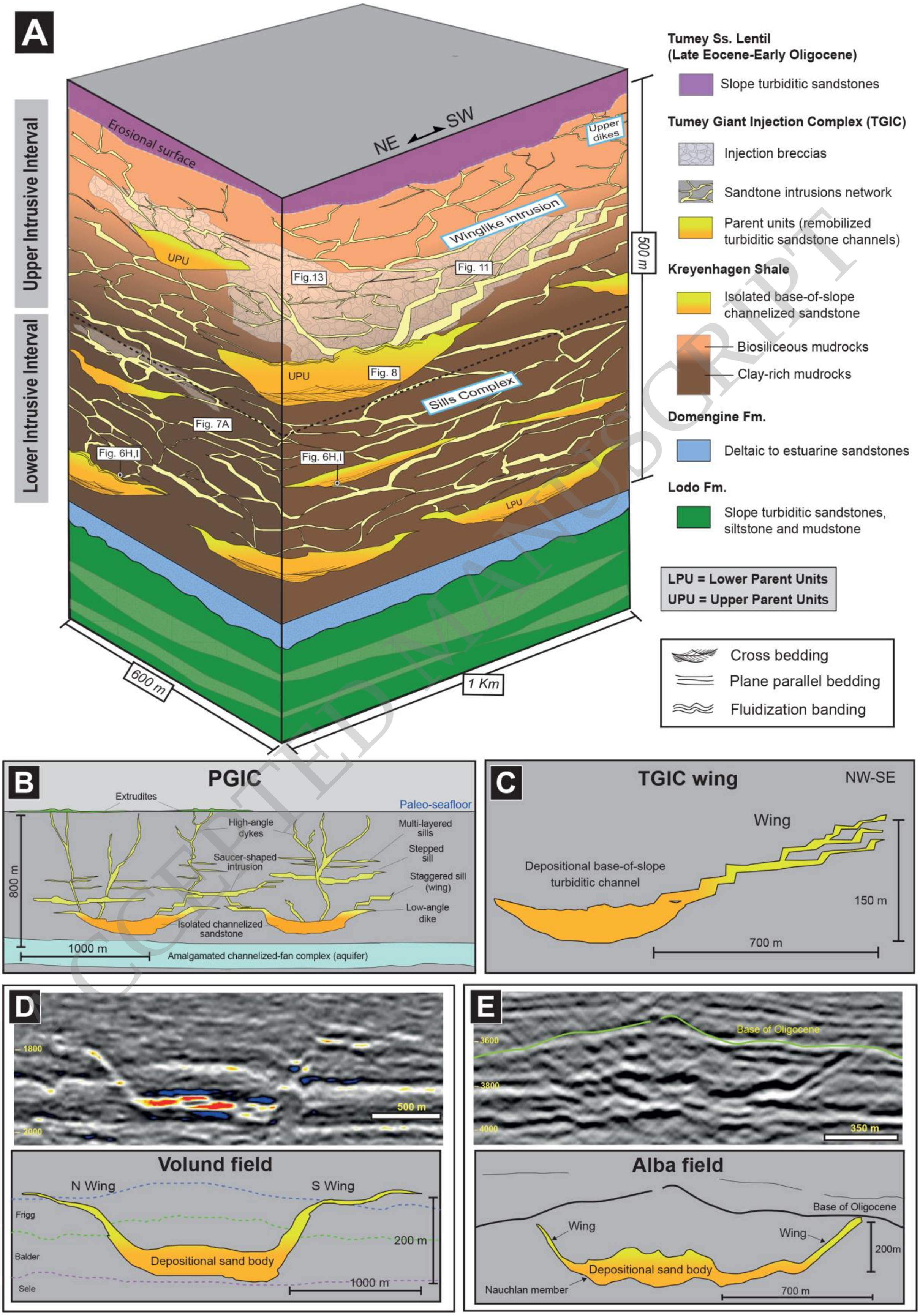
A
Upper Intrusive Interval
Lower Intrusive Interval
Erosional surface
NE
SW
Upper dikes
Winglike intrusion
UPU
Fig.13
Fig. 11
500 m
UPU
Fig. 8
Sills Complex
Fig. 7A
Fig. 6H,I
Fig. 6H,I
LPU
600 m
1 Km
Tumey Ss. Lentil
(Late Eocene-Early Oligocene)
Slope turbiditic sandstones
Tumey Giant Injection Complex (TGIC)
Injection breccias
Sandtone intrusions network
Parent units (remobilized turbiditic sandstone channels)
Kreyenhagen Shale
Isolated base-of-slope channelized sandstone
Biosiliceous mudrocks
Clay-rich mudrocks
Domengine Fm.
Deltaic to estuarine sandstones
Lodo Fm.
Slope turbiditic sandstones, siltstone and mudstone
LPU = Lower Parent Units
UPU = Upper Parent Units
Cross bedding
Plane parallel bedding
Fluidization banding
B
PGIC
Extrudites
Paleo-seafloor
High-angle dykes
Multi-layered sills
Stepped sill
Saucer-shaped intrusion
Staggered sill (wing)
Low-angle dike
Isolated channelized sandstone
800 m
1000 m
Amalgamated channelized-fan complex (aquifer)
C
TGIC wing
NW-SE
Wing
Depositional base-of-slope turbiditic channel
150 m
700 m
D
1800
2000
500 m
Volund field
N Wing
S Wing
Frigg
Balder
Sele
200 m
Depositional sand body
1000 m
E
3600
3800
4000
Base of Oligocene
350 m
Alba field
Base of Oligocene
Wing
Wing
200m
Depositional sand body
Nauchlan member
700 m

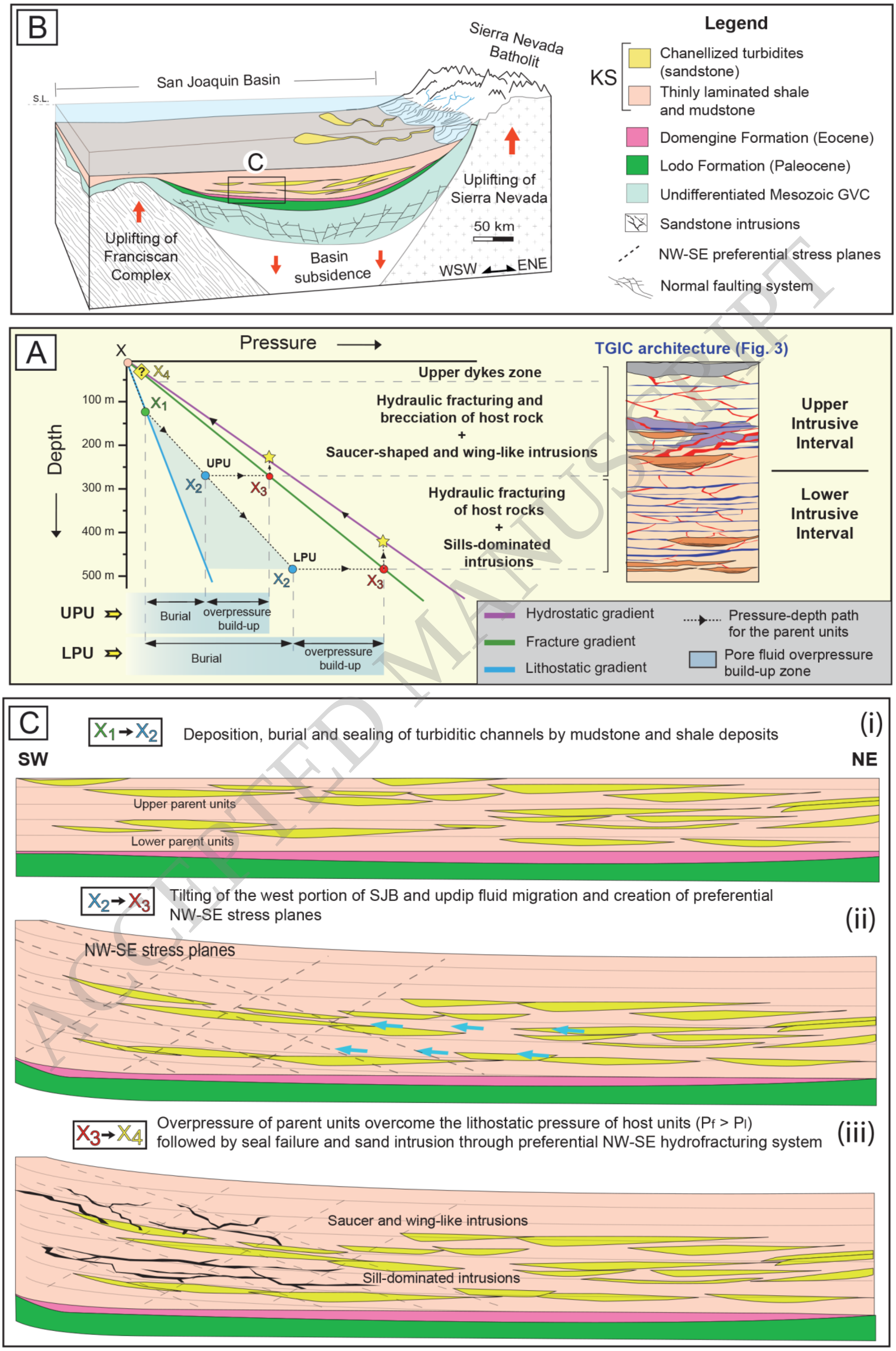
B
S.L.
San Joaquin Basin
Sierra Nevada Batholit
C
Uplifting of Sierra Nevada
50 km
Uplifting of Franciscan Complex
Basin subsidence
WSW
ENE
Legend
KS
Chanellized turbidites (sandstone)
Thinly laminated shale and mudstone
Domengine Formation (Eocene)
Lodo Formation (Paleocene)
Undifferentiated Mesozoic GVC
Sandstone intrusions
NW-SE preferential stress planes
Normal faulting system
A
X
Pressure
Depth
100 m
200 m
300 m
400 m
500 m
?
X4
X1
X2
X3
UPU
LPU
Upper dykes zone
Hydraulic fracturing and brecciation of host rock
+
Saucer-shaped and wing-like intrusions
Hydraulic fracturing of host rocks
+
Sills-dominated intrusions
TGIC architecture (Fig. 3)
Upper Intrusive Interval
Lower Intrusive Interval
UPU
LPU
Burial
overpressure build-up
Burial
overpressure build-up
Hydrostatic gradient
Fracture gradient
Lithostatic gradient
Pressure-depth path for the parent units
Pore fluid overpressure build-up zone
C
SW
NE
X1→X2
Deposition, burial and sealing of turbiditic channels by mudstone and shale deposits
(i)
Upper parent units
Lower parent units
X2→X3
Tilting of the west portion of SJB and updip fluid migration and creation of preferential NW-SE stress planes
(ii)
NW-SE stress planes
X3→X4
Overpressure of parent units overcome the lithostatic pressure of host units (Pf > Pl) followed by seal failure and sand intrusion through preferential NW-SE hydrofracturing system
(iii)
Saucer and wing-like intrusions
Sill-dominated intrusions